

## Disclaimer

This Report, including the data and information contained in this Report, is provided to you on an “as is” and “as available” basis at the sole discretion of the Government of Alberta and subject to the terms and conditions of use below (the “Terms and Conditions”). The Government of Alberta has not verified this Report for accuracy and does not warrant the accuracy of, or make any other warranties or representations regarding, this Report. Furthermore, updates to this Report may not be made available. Your use of any of this Report is at your sole and absolute risk.

This Report is provided to the Government of Alberta, and the Government of Alberta has obtained a license or other authorization for use of the Reports, from:

Canadian Natural Upgrading Limited, Chevron Canada Limited and 1745844 Alberta Ltd., as owners, and Shell Canada Energy as operator, for the Quest Project

(collectively the “Project”)

Each member of the Project expressly disclaims any representation or warranty, express or implied, as to the accuracy or completeness of the material and information contained herein, and none of them shall have any liability, regardless of any negligence or fault, for any statements contained in, or for any omissions from, this Report. Under no circumstances shall the Government of Alberta or the Project be liable for any damages, claims, causes of action, losses, legal fees or expenses, or any other cost whatsoever arising out of the use of this Report or any part thereof or the use of any other data or information on this website.

### Terms and Conditions of Use

Except as indicated in these Terms and Conditions, this Report and any part thereof shall not be copied, reproduced, distributed, republished, downloaded, displayed, posted or transmitted in any form or by any means, without the prior written consent of the Government of Alberta and the Project.

The Government of Alberta’s intent in posting this Report is to make them available to the public for personal and non-commercial (educational) use. You may not use this Report for any other purpose. You may reproduce data and information in this Report subject to the following conditions:

- any disclaimers that appear in this Report shall be retained in their original form and applied to the data and information reproduced from this Report
- the data and information shall not be modified from its original form
- the Project shall be identified as the original source of the data and information, while this website shall be identified as the reference source, and
- the reproduction shall not be represented as an official version of the materials reproduced, nor as having been made in affiliation with or with the endorsement of the Government of Alberta or the Project

By accessing and using this Report, you agree to indemnify and hold the Government of Alberta and the Project, and their respective employees and agents, harmless from and against any and all claims, demands, actions and costs (including legal costs on a solicitor-client basis) arising out of any breach by you of these Terms and Conditions or otherwise arising out of your use or reproduction of the data and information in this Report.

Your access to and use of this Report is subject exclusively to these Terms and Conditions and any terms and conditions contained within the Report itself, all of which you shall comply with. You will not use this Report for any purpose that is unlawful or prohibited by these Terms and Conditions. You agree that any other use of this Report means you agree to be bound by these Terms and Conditions. These Terms and Conditions are subject to modification, and you agree to review them periodically for changes. If you do not accept these Terms and Conditions you agree to immediately stop accessing this Report and destroy all copies in your possession or control.

These Terms and Conditions may change at any time, and your continued use and reproduction of this Report following any changes shall be deemed to be your acceptance of such change.

If any of these Terms and Conditions should be determined to be invalid, illegal or unenforceable for any reason by any court of competent jurisdiction then the applicable provision shall be severed and the remaining provisions of these Terms and Conditions shall survive and remain in full force and effect and continue to be binding and enforceable.

These Terms and Conditions shall: (i) be governed by and construed in accordance with the laws of the province of Alberta and you hereby submit to the exclusive jurisdiction of the Alberta courts, and (ii) ensure to the benefit of, and be binding upon, the Government of Alberta and your respective successors and assigns.

APPENDIX D: BIOGENIC SOIL GAS FLUX REPORT



## Heavy Oil

### Controlled Document

Quest CCS Project

## Baseline data and analysis of biogenic flux of CO<sub>2</sub> across Quest approval area

<b>Project</b>	Quest CCS Project
<b>Document Title</b>	Baseline data and analysis of biogenic flux of CO <sub>2</sub> across Quest approval area
<b>Document Number</b>	07-3-ZE-7180-0016
<b>Document Revision</b>	01
<b>Document Status</b>	Final
<b>Document Type</b>	ZE7180- Other Report
<b>Control ID</b>	
<b>Owner / Author</b>	Luc Rock (includes contributions from Golder Associates Ltd, the University of British Columbia / University of Victoria, and the Shell Projects and Technology (P&T) Soil and Groundwater and BioDomain teams)
<b>Issue Date</b>	2015-01-21
<b>Expiry Date</b>	None
<b>ECCN</b>	EAR 99
<b>Security Classification</b>	Unrestricted
<b>Disclosure</b>	None

*Revision History shown on next page*




**Revision History**

**REVISION STATUS**

**APPROVAL**

Rev.	Date	Description	Originator	Reviewers	Approver
00	2014-12-23	Final for revision	Luc Rock	Matt Lahvis, Sarah Kassam, Sean McFadden	Sean McFadden
01	2015-01-21	Final version	Luc Rock	Matt Lahvis, Sarah Kassam, Sean McFadden	Sean McFadden
<p>All signed originals will be retained by the UA Document Control Center and an electronic copy will be stored in Livelink</p>					

**Signatures for this revision**

Date	Role	Name	Signature or electronic reference (email)
2015-01-23	Senior HSSE consultant (SME)	Matt Lahvis	ML_AER CO2 report.msg 
2015-01-26	Quest MMV coordinator	Sarah Kassam	SK_AER CO2 report.msg 
2015-01-21	Quest subsurface manager	Sean McFadden	SMcF_AER CO2 report.msg 

**Summary**

This report describes and discusses sampling activities undertaken across the Quest sequestration lease area to gather data on biogenic flux of CO2, and above ground / soil gas CO2 for the time period 2012 to 2014.

**Keywords**

QUEST, biogenic CO2 flux, soil gas, CO2 composition, isotopes

Baseline data and analysis of biogenic flux of CO2 across Quest approval area		01
Heavy Oil		
-		

# Baseline data and analysis of biogenic flux of CO<sub>2</sub> across Quest approval area

---

Luc Rock, December 2014

## Executive Summary

This report is provided in response to Condition 15) a) in the AER (ERCB) application approval referenced in the Carbon Dioxide Disposal Approval No. 11837A (the "Approval"), issued on August 24<sup>th</sup> 2012 to Shell Canada Limited. Condition 15) a) asked for baseline data and analysis of biogenic flux of CO<sub>2</sub> in different soil types throughout the approval area. A comprehensive dataset has been acquired with regards to the biogenic flux of CO<sub>2</sub> over the course of 2012, 2013, and 2014. Key sampling activities related to the Quest HBMP (Hydrosphere Biosphere Monitoring Plan), which included soil surface CO<sub>2</sub> flux measurements and soil gas data collection from the main land use types encountered within the Quest Sequestration Lease Area (SLA). Additional sampling activities included collection of eddy covariance data to assess CO<sub>2</sub> flux at injection pad 08-19-059-20W4, as well as in-situ field measurements including soil gas probes, CO<sub>2</sub> flux chambers, and a walk-over survey. The aim of this report is to describe the various sampling activities undertaken within the Quest SLA to gather data on the biogenic flux of CO<sub>2</sub> and to discuss the findings from those campaigns.

# Table of Contents

- Executive Summary..... 1
- 1. Introduction ..... 6
- 2. Description of sampling activities ..... 7
  - 2.1. HBMP ..... 7
    - 2.1.1. Sampling sites ..... 7
    - 2.1.2. Materials and Methods..... 10
  - 2.2. Eddy co-variance ..... 11
    - 2.2.1. Sampling sites ..... 11
    - 2.2.2. Materials and Methods..... 11
  - 2.3. In-situ field measurements ..... 12
    - 2.3.1. Sampling sites ..... 12
    - 2.3.2. Materials and Methods..... 13
- 3. Results and Discussion ..... 14
  - 3.1. CO<sub>2</sub> flux data ..... 14
    - 3.1.1. “off-pad” measurements ..... 14
    - 3.1.2. “On-pad” measurements ..... 19
  - 3.2. Above ground atmosphere and soil gas data ..... 24
  - 3.3. CO<sub>2</sub> walk-over survey data ..... 30
- 4. Synopsis ..... 34
- 5. Acknowledgements..... 34

## List of Figures

Figure 2.1: Map of plots (small squares with line pointing to site ID) used for soil surface CO <sub>2</sub> flux and soil gas collection during the 2012 to 2014 HBMP sampling campaigns. Refer to Table 2.2 for further details on the sampled plots. (modified from Golder Associates Ltd) .....	8
Figure 2.2: Map schematics of July 2014 in-situ field sampling on and near the three injection well pad areas (pad 7-11: 7-11-59-20W4; pad 5-35: 5-35-21-W4; pad 8-18: 8-19-59-20W4). .....	13
Figure 3.1: Box plot of soil surface CO <sub>2</sub> flux ( $\mu\text{mol m}^{-2} \text{s}^{-1}$ ) versus season for all data collected as part of the 2012-2014 HBMP sampling activities.....	15
Figure 3.2: Box plot of soil surface CO <sub>2</sub> flux ( $\mu\text{mol m}^{-2} \text{s}^{-1}$ ) versus season split by sampling year (2012-rose color; 2013-blue color; 2014-green color) for all data collected as part of the 2012-2014 HBMP sampling activities. ....	16
Figure 3.3: Box plot of soil surface CO <sub>2</sub> flux ( $\mu\text{mol m}^{-2} \text{s}^{-1}$ ) versus land use type split by season for all data collected as part of the 2012-2014 HBMP sampling activities. ....	16
Figure 3.4: Box plot of Fall soil surface CO <sub>2</sub> flux ( $\mu\text{mol m}^{-2} \text{s}^{-1}$ ) versus land use type split by year for all data collected as part of the 2012-2014 HBMP sampling activities. ....	17
Figure 3.5: Box plot of soil surface CO <sub>2</sub> flux ( $\mu\text{mol m}^{-2} \text{s}^{-1}$ ) versus soil type split by season for all data collected as part of the 2012-2014 HBMP sampling activities. Note that for some sites, soil type is not available (referred to as not_ass...), and chernoz... refers to chernozem.....	18
Figure 3.6: Box plot of soil surface CO <sub>2</sub> flux ( $\mu\text{mol m}^{-2} \text{s}^{-1}$ ) versus soil type split by sampling year for all data collected as part of the 2012-2014 HBMP sampling activities. Note that for some sites, soil type is not available (referred to as not_assessed). ....	18
Figure 3.7: Box plot of soil surface CO <sub>2</sub> flux ( $\mu\text{mol m}^{-2} \text{s}^{-1}$ ) versus sampling site for land use type 'annual crop' split by sampling year (2012-rose color; 2013-blue color; 2014-green color) for all data collected as part of the 2012-2014 HBMP sampling activities. ....	19
Figure 3.8: Half-hourly eddy-covariance measurements of CO <sub>2</sub> flux (FC) for May 2012 to October 2014 at pad 8-19. The EC sensors moved from the southwest quadrant to the southeast quadrant and lowered from the 2-m height to the 1-m height on 4 July 2014. (from the University of British Columbia / University of Victoria Eddy co-variance work) .....	20
Figure 3.9: a) CO <sub>2</sub> fluxes measured by the eddy-covariance system mounted at the 2-m height on the post in the southwest sector of pad 8-19 in July 2013; b) Expanded view of the eddy-covariance CO <sub>2</sub> fluxes for July 25-29, 2013 showing strong negative daytime fluxes (photosynthesis) and strong	



positive nighttime fluxes (respiration). (from the University of British Columbia / University of Victoria Eddy co-variance work)..... 21

Figure 3.10: Median CO<sub>2</sub> fluxes ( $\mu\text{mol m}^{-2} \text{s}^{-1}$ ) as a function of radial distance from injection well at Well Pad 5-35 and 8-19 measured using the a) Picarro CRDS and b) LI-COR IRGA. Nb: extend of vertical black lines crossing median values represent min and max flux values recorded. (after Shell Projects and Technology (P&T) Soil and Groundwater and BioDomain teams)..... 21

Figure 3.11: Daytime flux footprint (contours indicate % of flux footprint) determined for typical daytime values of climatic and site variables (e.g. wind speed, measurement height). Green circle indicates radial extend of the surface flux chambers setup discussed under section 2.3. Note that the nighttime flux footprint is similar (data not shown). (from the University of British Columbia / University of Victoria Eddy co-variance work) ..... 23

Figure 3.12: Median  $\delta^{13}\text{C-CO}_2$  values (‰) (determined using Keeling plot) as a function of radial distance from injection well at Well Pads 5-35 and 8-19 measured using the Picarro CRDS. Nb: extend of vertical black lines crossing median values represent min and max flux values. (from the Shell Projects and Technology (P&T) Soil and Groundwater and BioDomain teams)..... 24

Figure 3.13: Box plot of ambient air CO<sub>2</sub> concentration (ppmv) at 0.1 (rose color) and 1 (blue color) m elevation by season for all data collected as part of the 2012-2014 HBMP sampling activities..... 25

Figure 3.14: Box plot of ambient air CO<sub>2</sub> concentration (ppmv) at 0.1 (rose color) and 1 (blue color) m elevation by land use type for all data collected as part of the 2012-2014 HBMP sampling activities. Nb: broadleaf referred to as deciduous for box plots showing CO<sub>2</sub> flux data..... 25

Figure 3.15: Box plot of ambient air CO<sub>2</sub> concentration (ppmv) at 0.1 (rose color) and 1 (blue color) m elevation by soil type for all data collected as part of the 2012-2014 HBMP sampling activities. Nb: broadleaf referred to as deciduous for box plots showing CO<sub>2</sub> flux data; for some sites, soil type is not available (referred to as not\_ass...). ..... 26

Figure 3.16: Box plot of ambient air CO<sub>2</sub> concentration (ppmv) at 1 m elevation by season for the discrete ambient air samples collected as part of the 2012-2014 HBMP sampling activities. Shown as well are the concomitant in-field measurements from the GGA instrument. Nb: (... refers to (ppmv)). ..... 26

Figure 3.17: Cross-plot of soil gas CO<sub>2</sub> concentration (ppmv) measured by the GGA versus CO<sub>2</sub> concentration measured in the laboratory (ppmv) for all data collected as part of the 2012-2014 HBMP sampling activities. .... 28

Figure 3.18: Box plot of soil gas CO<sub>2</sub> concentration (ppmv) by season for all samples collected as part of the 2012-2014 HBMP sampling activities..... 28

Figure 3.19: Box plot of soil gas CO<sub>2</sub> concentration (ppmv) by soil type for all samples collected as part of the 2012-2014 HBMP sampling activities. Note that for some sites, soil type is not available (referred to as not\_asse...). ..... 29

Figure 3.20: Box plot of soil gas δ<sup>13</sup>C- CO<sub>2</sub> values (‰) by season for all samples collected as part of the 2012-2014 HBMP sampling activities. .... 29

Figure 3.21: Box plot of soil gas δ<sup>13</sup>C- CO<sub>2</sub> values (‰) by land use type for all samples collected as part of the 2012-2014 HBMP sampling activities. .... 30

Figure 3.22: Spatial plots of air data mapped to regular grid for Well Pad 5-35. (from the Shell Projects and Technology (P&T) Soil and Groundwater and BioDomain teams)..... 31

Figure 3.23: Spatial plots of air data mapped to regular grid for Well Pad 8-19. (from the Shell Projects and Technology (P&T) Soil and Groundwater and BioDomain teams)..... 32

Figure 3.24: Spatial plots of air data mapped to regular grid for Well Pad 7-11. (from the Shell Projects and Technology (P&T) Soil and Groundwater and BioDomain teams)..... 33

**List of Tables**

Table 2.1: Main land use types within Quest SLA and distribution of sampling site locations during 2013. 7

Table 2.1: Plots sampled as part of the HBMP a) soil gas and b) soil surface CO<sub>2</sub> flux sampling campaigns. Nb: ‘x’ denotes plot sampled; ^ refers to site next to one of the three injection well pad referred to as 5-35-59-21W4M, 8-19-59-20W4M, 7-11-59-20W4M on Figure 2.1. .... 9

## 1. Introduction

As part of the Carbon Dioxide Disposal Approval No. 11837A (the “Approval”), issued on August 24<sup>th</sup> 2012 to Shell Canada Limited, condition 15) a) referred to inclusion of a report on ‘*baseline data and analysis of biogenic flux of CO<sub>2</sub> in different soil types throughout the approval area*’ within the 3<sup>rd</sup> Annual Status report. The key activity to address this condition is related to the Quest HBMP monitoring activities. The HBMP is the Hydrosphere and Biosphere Monitoring Plan implemented as part of the Quest MMV plan, with a focus on the baseline (pre-injection) monitoring activities. A couple of additional monitoring activities, however, provide additional and current state-of-the-art technology data.

This report is provided in response to Condition 15)a) in the AER (ERCB) application approval referenced in the Carbon Dioxide Disposal Approval No. 11837A issued to Shell Canada Limited. The report addresses the following two specific objectives:

- a. Description of sampling activities undertaken to gather data on biogenic flux of CO<sub>2</sub> across the Quest SLA for the time period 2012 to 2014.
- b. Discussion of the results obtained.

Hence, this report is organized using the following structure: Section 2 will describe the sampling activities undertaken, which fall into three categories: i) HBMP, ii) Eddy co-variance, and iii) in-situ field measurements. Section 3 presents and discusses the results obtained and split by type, namely CO<sub>2</sub> flux data (covers categories i, ii, iii); soil gas data (covers categories i, iii); CO<sub>2</sub> survey data (covers category iii). Section 4 provides a brief synopsis of the work presented.

Note that the work presented in this report is based upon contractual and partly collaborative work between Shell Canada and Golder Associates Ltd for HBMP, the University of British Columbia / University of Victoria for Eddy co-variance, and the Shell Projects and Technology (P&T) Houston Soil and Groundwater and BioDomain teams for the in-situ field measurements.

## 2. Description of sampling activities

### 2.1. HBMP

The Quest HBMP includes monitoring activities related to the hydrosphere and biosphere. With regards to the latter, an extensive soil gas and soil surface CO<sub>2</sub> flux sampling program was undertaken during 2012 (one season), 2013 (every season) and 2014 (every season) in order to gain an understanding of the magnitudes and temporal / spatial variability of those parameters in the Quest SLA.

#### 2.1.1. Sampling sites

It is expected that soil gas composition and soil surface CO<sub>2</sub> flux will vary across the landscape, as it depends upon a range of factors such as land use type (e.g. forest versus agriculture), or management type within an agricultural setting (e.g. cereal versus legume, or unamended soil versus fertilized soil with synthetic nitrogen). In turn, it is difficult to capture all possible scenarios; however, sampling sites were selected to ensure data were collected from the main land use types encountered within the SLA as illustrated for 2013 (Table 2.1).

*Table 2.1: Main land use types within Quest SLA and distribution of sampling site locations during 2013.*

	<b>Area (ha)</b>	<b>% of Total Project Area</b>	<b># of field plots (2013)</b>	<b>% of field plots (2013)</b>
<b>Annual Crop</b>	132,400	35%	5	33%
<b>Broadleaf Forest</b>	86,700	23%	3	20%
<b>Pasture</b>	85,300	23%	3	20%
<b>Coniferous Forest</b>	37,400	10%	2	13%
<b>Wetland</b>	27,000	7%	2	13%
<b>Developed</b>	6,500	2%	0	0%
<b>Water</b>	4,600	1%	0	0%
<b>Total</b>	380,000	100%	15	100%

A total of 21 plots were visited over the course of the sampling period between 2012 and 2014. Figure 2.1 shows the location of the plots that were part of the HBMP for soil surface CO<sub>2</sub> flux and soil gas collection. Table 2.2 provides further details regarding what samples were collected and when at the various plots. As shown in Table 2.2, some sites were excluded from the sampling program, while others were added. This was due to site accessibility issues, redundancy (same soil type or land-use between sites), and goal to ensure representative coverage of various land-use types within the SLA as illustrated for 2013 in Table 2.1.

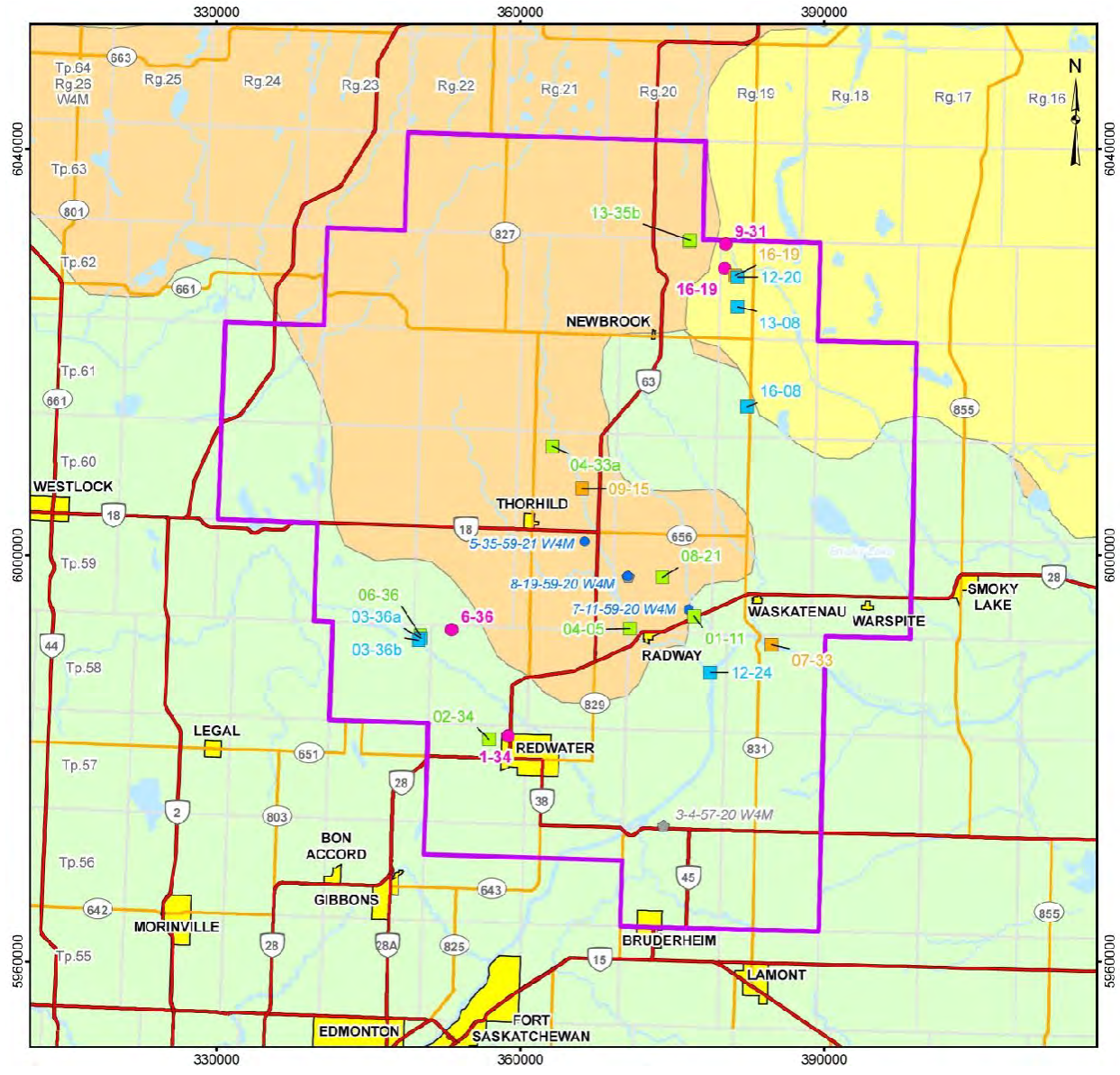


Figure 2.1: Map of plots (small squares with line pointing to site ID) used for soil surface CO<sub>2</sub> flux and soil gas collection during the 2012 to 2014 HBMP sampling campaigns. Refer to Table 2.2 for further details on the sampled plots. (modified from Golder Associates Ltd)

Table 2.1: Plots sampled as part of the HBMP a) soil gas and b) soil surface CO<sub>2</sub> flux sampling campaigns. Nb: 'x' denotes plot sampled; ^ refers to site next to one of the three injection well pad referred to as 5-35-59-21W4M, 8-19-59-20W4M, 7-11-59-20W4M on Figure 2.1.

a)	Site ID	Fall 2012	Spring 2013	Summer 2013	Fall 2013	Winter 2014	Spring 2014	Summer 2014	Fall 2014
"adjacent to injection wells"	IW05-35 ^	x	x	x	x	x	Probe Flooded	x	x
	IW05-35 ^	x	x	x	x	x	Probe Flooded	Probe Flooded	Probe Flooded
	IW05-35 ^	x	x	x	x	Probe Frozen	Probe Flooded	Probe Flooded	Probe Flooded
	IW07-11 ^	x	x	x	x	Probe Frozen	x	x	x
	IW07-11 ^	x	x	x	x	Probe Frozen	x	x	x
	IW07-11 ^	x	x	x	x	Probe Frozen	x	x	x
	IW08-19 ^	No access	x	Probe Removed	x	x	Probe Flooded	x	x
	IW08-19 ^	No access	x	Probe Removed	x	x	x	x	x
IW08-19 ^	No access	x	Probe Removed	x	x	Probe Flooded	x	x	
"regionally distributed sites throughout Quest SLA"	01-11	x	x	x	x	Ground Frozen	x	x	x
	02-34	x	x	x	x	Ground Frozen	Probe Flooded	x	x
	03-36a	Added Spring '13	x	Probe Removed	x	x	x	x	x
	03-36b	Added Spring '13	Probe Wet	Probe Wet	x	x	x	x	x
	04-05	x	x	x	x	Ground Frozen	x	x	x
	04-33a	x	Probe Wet	Probe Wet	x	x	x	x	x
	04-33b	Split Spring '13	x	x	x	x	x	x	x
	06-36	x	Probe Wet	Probe Wet	x	Ground Frozen	Probe Flooded	Probe Flooded	Probe Flooded
	07-33	x	Discontinued						
	08-21	x	x	Probe Wet	x	Ground Frozen	x	x	x
	09-15	x	Discontinued						
	12-20	Added Spring '13	x	x	x	Leaking Probe	x	x	x
	12-24	Added Summer '13	Added Summer '13	x	x	x	x	x	x
	13-08	Added Spring '13	Probe Wet	x	x	Ground Frozen	x	x	x
	13-35a	Split Spring '13	Probe Wet	x	x	x	x	x	x
	13-35b	x	Probe Wet	Probe Wet	x	Could not locate probe	Probe Flooded	x	x
	16-08	Added Summer '13		Probe Wet	x	Ground Frozen	x	x	x
16-19	x	Discontinued							

b)	Site ID	Fall 2012	Winter 2013	Spring 2013	Summer, Fall 2013	Winter, Spring Summer, Fall 2014
"adjacent to injection wells"	IW05-35 ^	x	x	x	x	x
	IW07-11 ^	x	x	x	x	x
	IW08-19 ^		x	x	x	x
"regionally distributed sites throughout Quest SLA"	01-11	x	x	x	x	x
	02-34	x	x	x	x	x
	03-36a		added spring 2013	x	x	x
	03-36b		added spring 2013	x	x	x
	04-05	x	x	x	x	x
	04-33a	x	Snow too deep	x	x	x
	04-33b	x	x	x	x	x
	06-36	x	No access	x	x	x
	07-33	x				
	08-21	x	x	x	x	x
	09-15	x				
	12-20		added spring 2013	x	x	x
	12-24		Added summer 2013		x	x
	13-08		Added summer 2013		x	x
	13-35a	x	x	x	x	x
	13-35b	x	x	x	x	x
	16-08		added spring 2013	x	x	x
16-19	x					

### 2.1.2. Materials and Methods

During each field sampling campaign, soil gas compositional data and soil surface CO<sub>2</sub> flux measurements gas were collected whenever possible (e.g. frozen soil may limit soil gas sampling; Table 2.2). Discrete measurements were taken every season at the various sampling sites whenever possible from 2012 to 2014, with the first sampling event in Fall 2012 to address temporal and spatial variability in CO<sub>2</sub> measurements.

Soil surface CO<sub>2</sub> flux measurements were taken at 3 randomly chosen sampling points located within 1 hectare of homogeneous soil/vegetation type. The 3 randomly chosen sampling points, selected during the first visit of a particular sampling site (plot, e.g. 01-11), were then repeatedly sampled every season thereafter. Soil surface CO<sub>2</sub> flux measurements were obtained using a field-deployable LiCOR Model 8100A CO<sub>2</sub> flux survey chamber, at a frequency of about 6 to 10 three minute long replicate measurements (1 minute purge, 2 minutes sampling) at each collar. A soil moisture probe and a soil temperature probe were part of the setup. In the field, the LiCOR chamber was placed upon 20 cm diameter soil collars, which were installed 24 hours before the measurement period. Long grass and other vegetation that may interfere with the closing and sealing of the chamber on the rim of the collar were trimmed using scissors during collar installation. No vegetation, leaf litter or other material was removed from inside the collar unless it interfered with the instrument, i.e., all efforts were made to minimize disturbance to the surface being analyzed.

Soil gas samples were collected from three depths down to about 2 m below the ground surface at each “adjacent to injection wells” site, and at a single depth at each of the “regionally distributed sites throughout Quest SLA” sites. Soil gas sampling probes were installed close to the center of the cluster represented by the surface CO<sub>2</sub> flux collars. The sampling program included concurrent sampling of soil gas samples and surface flux. A Model 915-0011 ultra-portable field deployable Greenhouse Gas Analyzer (GGA) (Los Gatos Research, California) for measuring CO<sub>2</sub>, H<sub>2</sub>O and CH<sub>4</sub>, was used during sample collection to ensure probes were purged of air and that there was no short-circuiting of atmospheric air into the probe post sample collection. Samples were collected in either glass bottles or pre-evacuated SUMMA canisters for off-site laboratory analysis. The laboratory analytes included (if possible):

- Compositional: CO<sub>2</sub>, C<sub>1</sub> to C<sub>10+</sub>, N<sub>2</sub>, O<sub>2</sub>, He
- Isotopic: δ<sup>13</sup>C-CO<sub>2</sub>, δ<sup>13</sup>C-CH<sub>4</sub> and δ<sup>13</sup>C-C<sub>2+</sub>, δ<sup>2</sup>H-CH<sub>4</sub>.

Nb: the focus in this report will be on CO<sub>2</sub> (concentration, flux, isotopic composition).



Besides collecting data for soil gas, samples from the above ground atmosphere were also collected. Atmospheric gas samples were collected using two methods: a) discrete flask samples taken at a height of 1m above ground for offsite laboratory analysis (as described above), and b) in-situ real time measurements at a height of 0.1 and 1 m above ground using the field deployable GGA.

## **2.2. Eddy co-variance**

### **2.2.1. Sampling sites**

Eddy co-variance (EC) measurements have been taken on injection pad 08-19-059-20W4 since April 2012 until present. Initially, the EC system was installed on a mast 2 m above the ground close to a meteorological weather station in the SW corner of the pad. In early July 2014, the system was moved to a tripod in the SE corner of the pad and installed at a 1-m height. This was done in order to ensure that the footprint of the EC measurements lay almost entirely within the injection pad 08-19-059-20W4 area, as presented in section 3.1. Note that EC system height installation influences the surficial area away from the EC system represented by the data collected.

### **2.2.2. Materials and Methods**

Since April 2012, continuous high-frequency (HF) measurements have included the three components of the wind vector and air temperature, CO<sub>2</sub> and H<sub>2</sub>O using an infrared gas analyser (IRGA) (model LI-7200, LI-COR, Inc., Lincoln, NE). Meteorological data included air temperature, relative humidity, barometric pressure, wind speed and direction, shortwave (i.e. solar) irradiance, and rainfall. Soil temperature and moisture were also measured.

The same meteorological measurements were continued after the physical relocation of the EC system, except for the addition of three soil heat flux plates. Half-hourly covariances of the sonic air temperature, H<sub>2</sub>O and CO<sub>2</sub> mixing ratios with the vertical wind velocity ( $w$ ) were used to calculate CO<sub>2</sub> (FC) fluxes. In September 2014, an additional instrument was installed to support interpretation of the EC data, namely a four-way net radiometer.

Quality EC measurements have been collected; however, there is some uncertainty in the May 2012 to June 2014 CO<sub>2</sub> flux values for specific parts of the land surface (e.g. pad vs crop). The reason for this is the combination of pad and crop surfaces contributing to the EC system and the proximity of the berms/nearby Aspen trees affected the fluxes for the majority of the wind directions. With regards to the EC measurements taken at the 1m tripod, data were compromised during the July-August 2014 time



period due to the presence of temporary infrastructure on the pad which interfered with the air movement.

### **2.3. In-situ field measurements**

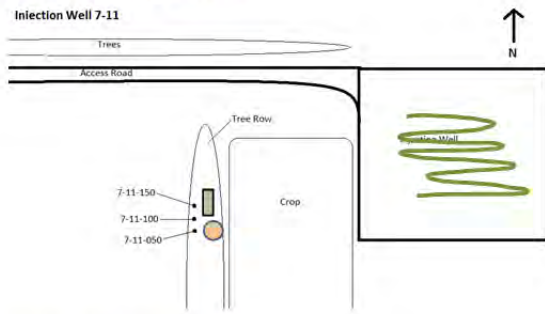
In July 2014, a 3-day field campaign was undertaken to collect in-situ field measurements on CO<sub>2</sub> flux, concentration and isotopic composition using current state-of-the-art field deployable instrumentation.

#### **2.3.1. Sampling sites**

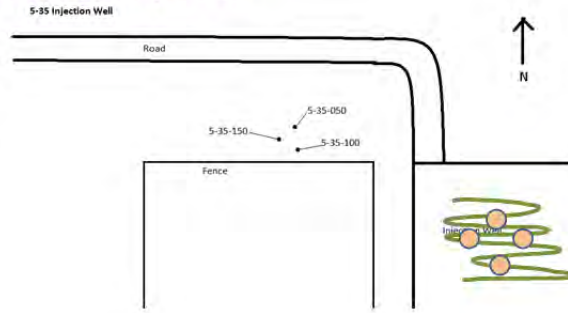
In-situ field measurements were focused on the injection well pad areas 07-11-059-20W4 (referred to as 7-11), 08-19-059-20W4 (referred to as 8-19) and 05-35-059-21W4 (referred to as 5-35), and nearby existing soil gas probes sampled as part of the HBMP. For location of the injection well pad areas, please refer to Figure 2.1. Sampling included walk-over surveys across the pads, soil gas probe sampling, and CO<sub>2</sub> flux chamber measurements (Fig. 2.2).

Surface flux chamber measurements included “off-pad” and “on-pad” sampling sites, to capture differences between the well pad and surrounding area, with the following configuration. For the “off-pad” measurements, a single collar for placing the automated LiCOR flux chamber was positioned near the existing soil gas probes for 7-11 and 8-19, close to the center of the soil gas probes layout. It was not possible to collect “off-pad” measurements at 5-35 due to time constraints. For the “on-pad” measurements, collars were placed in a radial configuration around the injection wells at 8-19 and 5-35. The radial configuration corresponded to 4 linear lines oriented 90deg to each other and pointing approximately to the N, E, S and W. In each linear direction, the collars were placed at approximately 5, 10, 20 and 35 ft (or 1.5, 3, 6 and 10.5m) away from the injector well. The soil gas sampling sites corresponded to the existing vertical soil gas probes that were installed as part of the HBMP.

### July 29<sup>th</sup>, 2014: pad 7-11



### July 30<sup>th</sup>, 2014: pad 5-35



### July 31<sup>st</sup>, 2014: pad 8-19

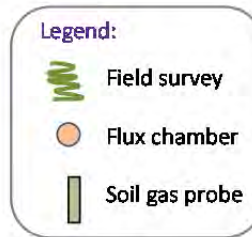
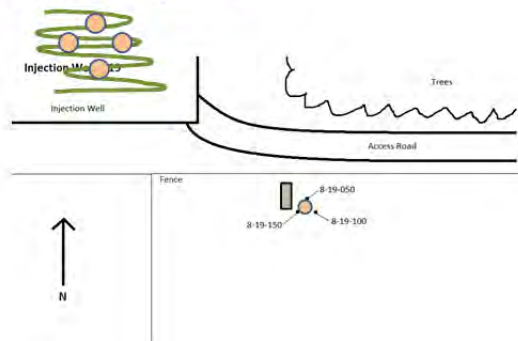


Figure 2.2: Map schematics of July 2014 in-situ field sampling on and near the three injection well pad areas (pad 7-11: 7-11-59-20W4; pad 5-35: 5-35-21-W4; pad 8-18: 8-19-59-20W4).

### 2.3.2. Materials and Methods

The mobile system used for the in-situ field measurements activities included a Picarro Mobile Kit and LiCOR 8100A. The LiCOR is equipped with an infrared gas analyzer (IRGA) for CO<sub>2</sub> gas analysis. The Picarro is equipped with a cavity ring-down spectrometer for <sup>12</sup>CO<sub>2</sub> and <sup>13</sup>CO<sub>2</sub> analyses. The system was also setup to collect discrete samples for laboratory analyses to cross-check the in-situ field analyses. The laboratory analyses have not been completed yet and will not be discussed further in this report. It should be noted though that controlled tests/analyses were done to check the performance of the mobile system prior to field deployment at the Quest sites.

For the surface flux measurements, the gases that accumulated in the chamber were circulated through a closed loop system including the LiCOR and Picarro analyzers as well as the flux chamber, which was positioned on top of a 20 cm diameter collar, similar to the ones used as part of the HBMP.

For the walk-over survey measurements, gas emitted at the soil surface were sampled via a tube connected to a survey wheel positioned at about 2cm from the ground surface. The tube was connected directly to the Picarro analyzer inlet. The system included a GPS unit, as well as an anemometer for measuring wind speed and direction. All data were collected continuously at about 7 second intervals

and aligned using Coordinated Universal Time (UTC) with an offset between physical location and gas concentration/isotope ratio to account for the delay between an air sample entering the tube at 2cm above the ground surface and it reaching the Picarro analyzer.

For the soil gas sampling, the setup was similar to the one used for the walk-over survey, the exception being that the gas sampling port was connected to the soil gas probe instead of the survey wheel.

With regards to data interpretation, Keeling plots (measured  $\delta^{13}\text{C}$  versus inverse of gas concentration) were used to determine the  $\delta^{13}\text{C}$ -CO<sub>2</sub> values (intercept of Keeling plot, which is  $\delta^{13}\text{C}$  value of respired gas in absence of atmospheric dilution) at a particular sampling location. For the walk-over surveys, the random spatial measurement locations from the mobile instrument were mapped onto a uniform rectangular grid at 2 m increments over the measurement area. For each grid point, a mean weighted value was calculated. The weighting process yields concentrations on a uniform rectangular grid averaged over the test duration.

## 3. Results and Discussion

### 3.1. CO<sub>2</sub> flux data

#### 3.1.1. “off-pad” measurements

A very comprehensive set of CO<sub>2</sub> flux data has been gathered during the 2012-2014 HBMP activities, which allowed assessment of both temporal and spatial variability in surface CO<sub>2</sub> flux across the Quest SLA. Flux data were obtained for 6 different land use types, including annual crop, coniferous forest, deciduous forest, meadow, pasture and wetland. Overall, soil surface CO<sub>2</sub> fluxes determined as part of the HBMP ranged from -0.42 to 24.09  $\mu\text{mol m}^{-2} \text{s}^{-1}$  (Fig. 3.1). Note that this range is based upon the mean CO<sub>2</sub> flux values determined for each sampling point (idem soil collar). There was very good agreement between the repeat analyses at a single collar, with the standard deviation being  $\leq 0.6 \mu\text{mol m}^{-2} \text{s}^{-1}$  in 90% of the cases.

A seasonal trend is clearly visible, as expected based biological activity, with the highest CO<sub>2</sub> fluxes being measured in the summer and the lowest in the winter (Figs. 3.1 and 3.2). As well, CO<sub>2</sub> fluxes for specific seasons were similar between sampling years (Figs. 3.2). Slight differences are expected among the same season for different sampling years to due climatic conditions leading to wetter or drier years, and hence influencing soil biological activity.

Differences in soil surface CO<sub>2</sub> fluxes were also observed between land use types (Fig. 3.3). Meadow, pasture and wetland tended to have higher CO<sub>2</sub> fluxes compared to annual crop or forest (coniferous, deciduous). It can also be noted that the relative difference in CO<sub>2</sub> flux magnitude was dependent upon season, with the largest differences between land use types being observed in the Spring and Summer seasons. Similar trends were observed among the season between individual sampling years, as illustrated for the Fall data in Figure 3.4.

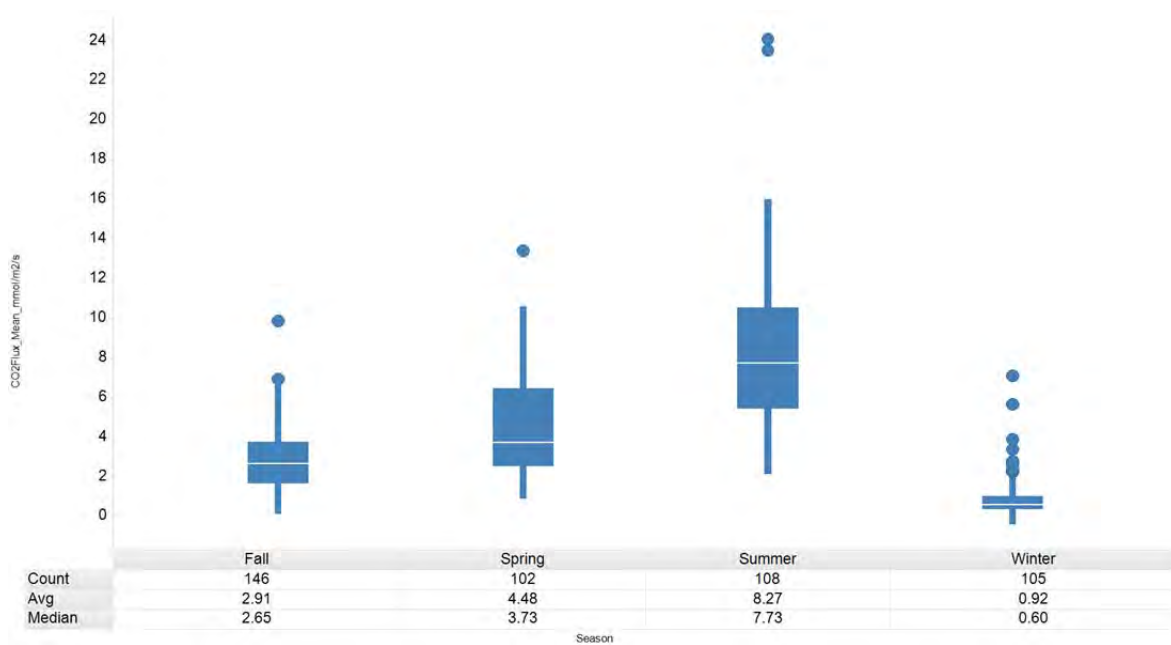


Figure 3.1: Box plot of soil surface CO<sub>2</sub> flux ( $\mu\text{mol m}^{-2} \text{s}^{-1}$ ) versus season for all data collected as part of the 2012-2014 HBMP sampling activities.

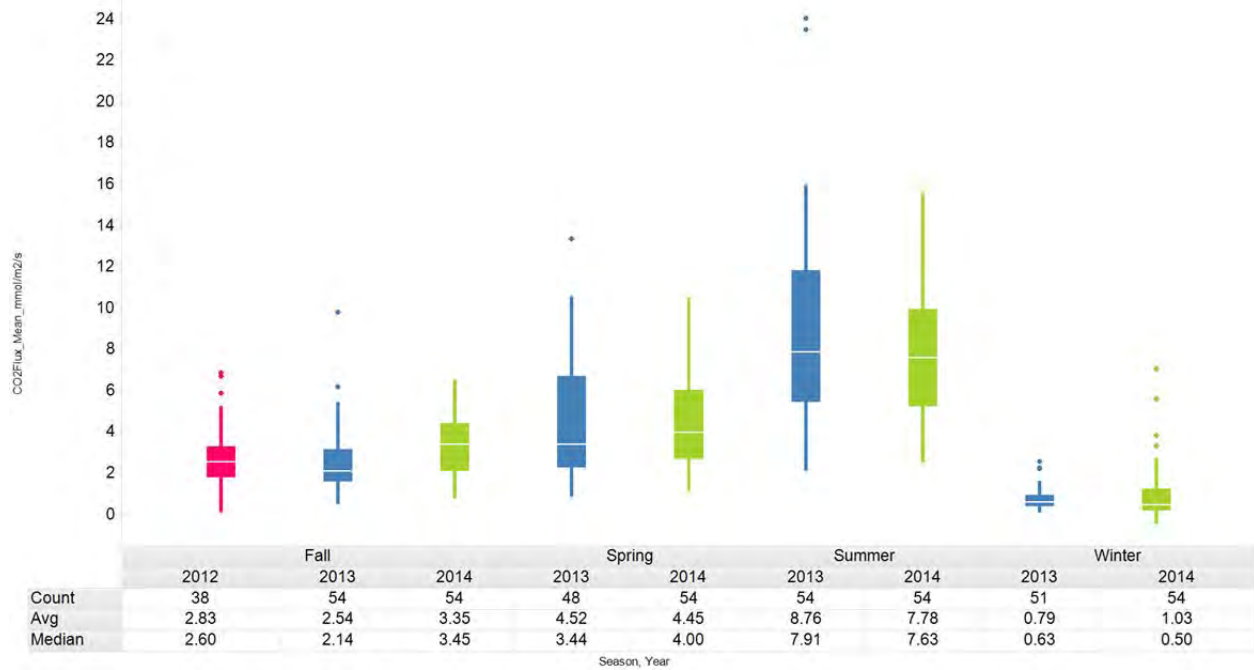


Figure 3.2: Box plot of soil surface CO<sub>2</sub> flux (µmol m<sup>-2</sup> s<sup>-1</sup>) versus season split by sampling year (2012-rose color; 2013-blue color; 2014-green color) for all data collected as part of the 2012-2014 HBMP sampling activities.

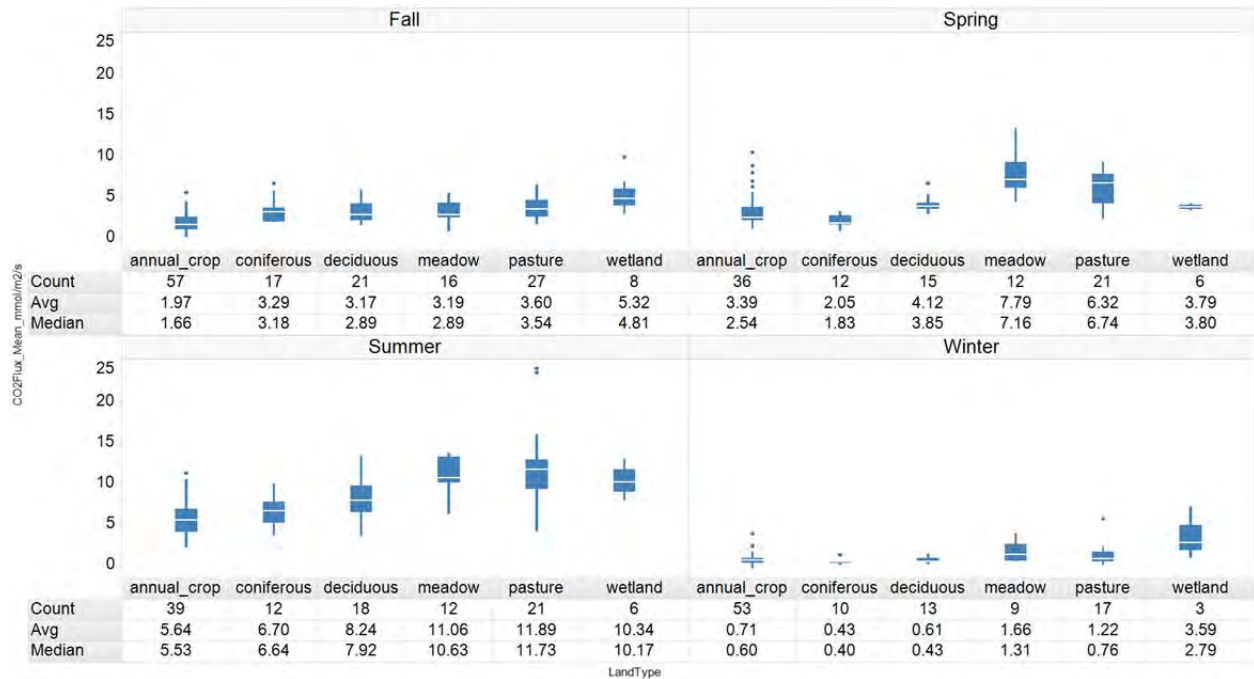


Figure 3.3: Box plot of soil surface CO<sub>2</sub> flux (µmol m<sup>-2</sup> s<sup>-1</sup>) versus land use type split by season for all data collected as part of the 2012-2014 HBMP sampling activities.



Figure 3.4: Box plot of Fall soil surface CO<sub>2</sub> flux ( $\mu\text{mol m}^{-2} \text{s}^{-1}$ ) versus land use type split by year for all data collected as part of the 2012-2014 HBMP sampling activities.

Besides information on land use types for the various sampling sites, soil type was also determined. A total of 7 soil types were assessed as part of the 2012-2014 sampling campaign (Fig. 3.5). These included brunisol, chernozem, gleysol, luvisol, organic, regosol, and solonetz. There is no clear difference in soil surface CO<sub>2</sub> fluxes between soil types over the course of the four seasons. An exception may be the soil type solonetz, which appears to have lower CO<sub>2</sub> fluxes during the Fall and Summer compared to the other soil types. When comparing the CO<sub>2</sub> fluxes by soil type between individual sampling years, regosol appears to have on average the highest CO<sub>2</sub> fluxes and solonetz the lowest CO<sub>2</sub> fluxes compared to the other soil types (Fig. 3.6).

Even though some differences were observed in CO<sub>2</sub> fluxes among soil types, the data suggest that land use type and season have a larger influence on CO<sub>2</sub> fluxes. It should also be noted, as would be expected, that there is considerable variability among sampling sites representing the same land use type. Figure 3.7 illustrates this variability in CO<sub>2</sub> fluxes among the 9 sampling sites that represent the land use type 'annual crop'.

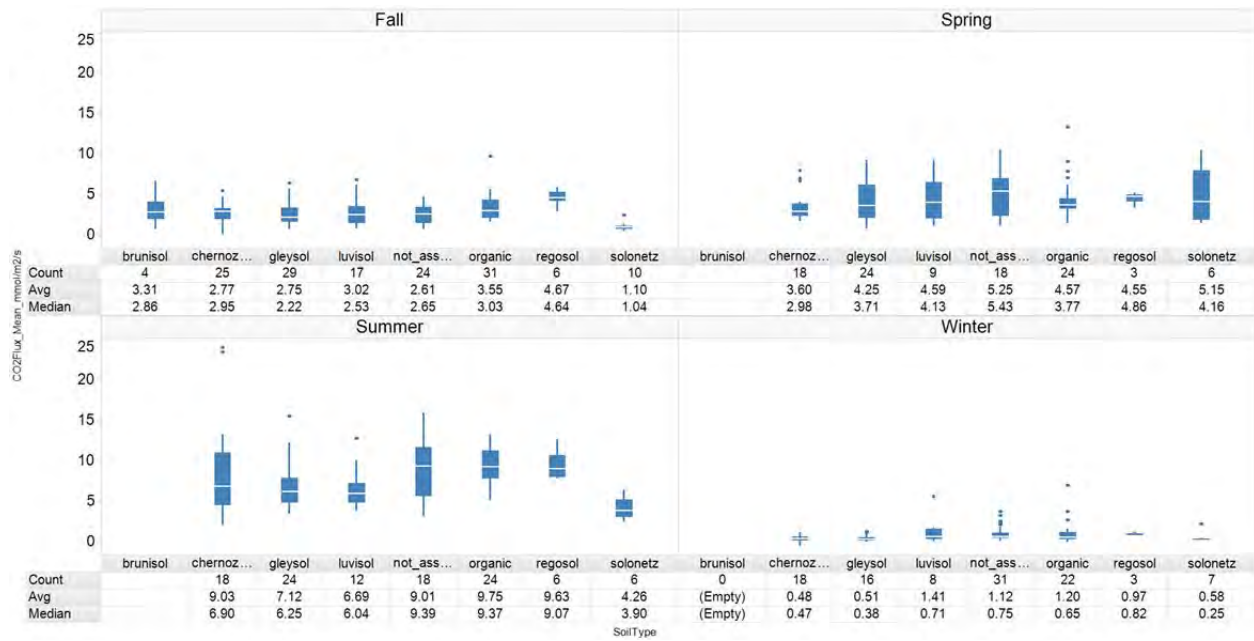


Figure 3.5: Box plot of soil surface CO<sub>2</sub> flux ( $\mu\text{mol m}^{-2} \text{s}^{-1}$ ) versus soil type split by season for all data collected as part of the 2012-2014 HBMP sampling activities. Note that for some sites, soil type is not available (referred to as not\_ass...), and chernoz... refers to chernozem.



Figure 3.6: Box plot of soil surface CO<sub>2</sub> flux ( $\mu\text{mol m}^{-2} \text{s}^{-1}$ ) versus soil type split by sampling year for all data collected as part of the 2012-2014 HBMP sampling activities. Note that for some sites, soil type is not available (referred to as not\_assessed).



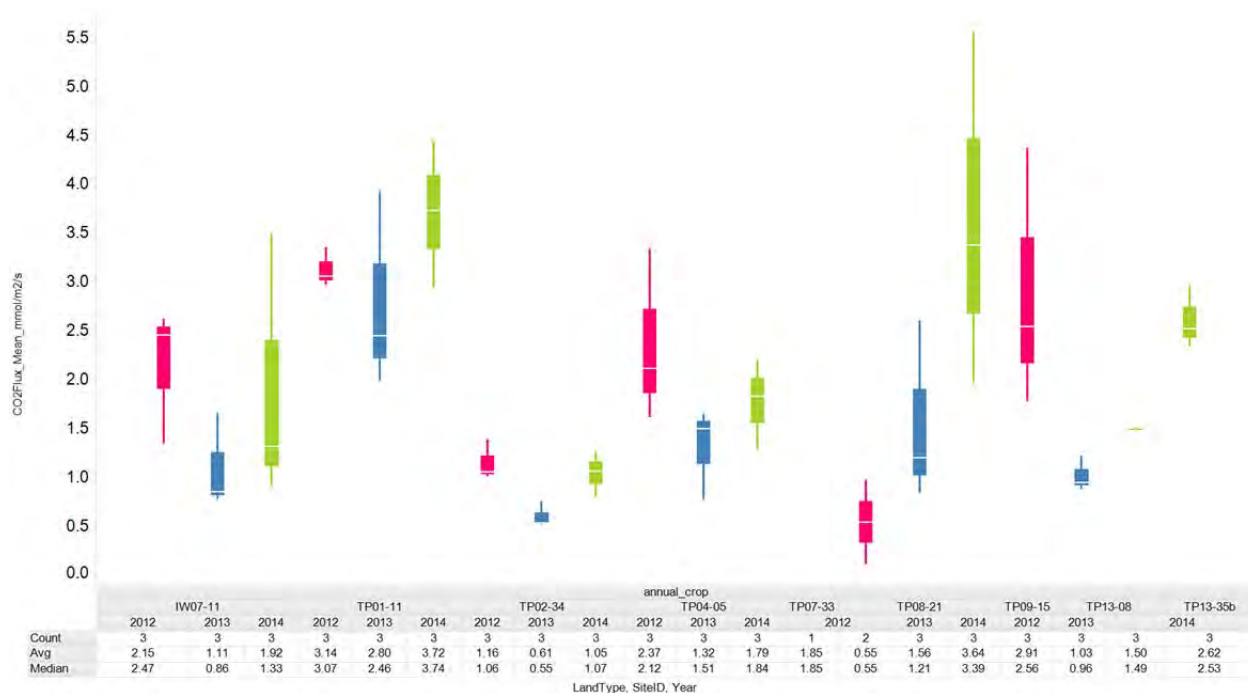


Figure 3.7: Box plot of soil surface CO<sub>2</sub> flux ( $\mu\text{mol m}^{-2} \text{s}^{-1}$ ) versus sampling site for land use type 'annual crop' split by sampling year (2012-rose color; 2013-blue color; 2014-green color) for all data collected as part of the 2012-2014 HBMP sampling activities.

Besides the very comprehensive HBMP dataset, a number of surface CO<sub>2</sub> flux measurements were taken as part of the July 2014 in-situ field sampling campaign described in section 2.3. The CO<sub>2</sub> fluxes determined at 8-19 and 7-11 ranged from 20.6 to 25.1 and 15.8 to 22.2  $\mu\text{mol m}^{-2} \text{s}^{-1}$  at 8-19 and 7-11, respectively, and fall within the CO<sub>2</sub> flux range determined for the HBMP. During measurement of the CO<sub>2</sub> flux, the  $\delta^{13}\text{C-CO}_2$  was also determined and ranged from -26.7 to -22.6‰, which is consistent with C3 vegetation and data collected as part of the HBMP (see section 3.2).

### 3.1.2. “On-pad” measurements

The CO<sub>2</sub> flux data determined as part of the EC setup at 8-19 ranged from  $< -20$  to  $> +20 \mu\text{mol m}^{-2} \text{s}^{-1}$  between May 2012 and October 2014 at 8-19 (Fig. 3.8), when including all data collected at the mast and tripod. Note that the EC measurements taken at the 2m mast (May 2012 to June 2014) reflect not only the pad footprint, but also contributions from crops outside the pad area. This is illustrated by the strong diurnal variations in CO<sub>2</sub> flux data (Fig. 3.9), especially during the growing season, reflecting nearby crop actively photosynthesizing during the day (decrease in CO<sub>2</sub> flux) and respiring at night (increase in CO<sub>2</sub> flux). Figure 3.9b shows the CO<sub>2</sub> flux values during the day were as low as  $-9 \mu\text{mol m}^{-2} \text{s}^{-1}$  indicating considerable CO<sub>2</sub> uptake, while at night the CO<sub>2</sub> flux values reached  $+7 \mu\text{mol m}^{-2} \text{s}^{-1}$  as would be expected in an actively growing crop. After the change of location and height of the EC sensors in July



2014, the diurnal variation of CO<sub>2</sub> flux was greatly reduced, as would be expected with the ‘flux’ footprint being restricted mainly to the pad area. The extremely high and low values of CO<sub>2</sub> flux between May 2012 and June 2014, prior to the change in the EC system location in early July 2014, are likely due to the disturbance of the wind flow by the berms and possibly nearby Aspen trees.

The July 2014 to October 2015 data allowed assessment of the CO<sub>2</sub> flux representative of the pad area. During data interpretation, the EC data were screened using the high frequency wind direction data to ensure that data included were those where wind direction blew at least 80% of the time from the wind direction window that includes the pad surface (ranging from 250° clockwise to 90°). The data indicated that CO<sub>2</sub> flux from pad 8-19 is small ( $< 0.3 \mu\text{mol m}^{-2} \text{s}^{-1}$ ) and suggest that the CO<sub>2</sub> observed likely has a source (probably remnant organic matter) deep enough that it is unaffected by changes in soil temperature and moisture measured at 3-cm depth.

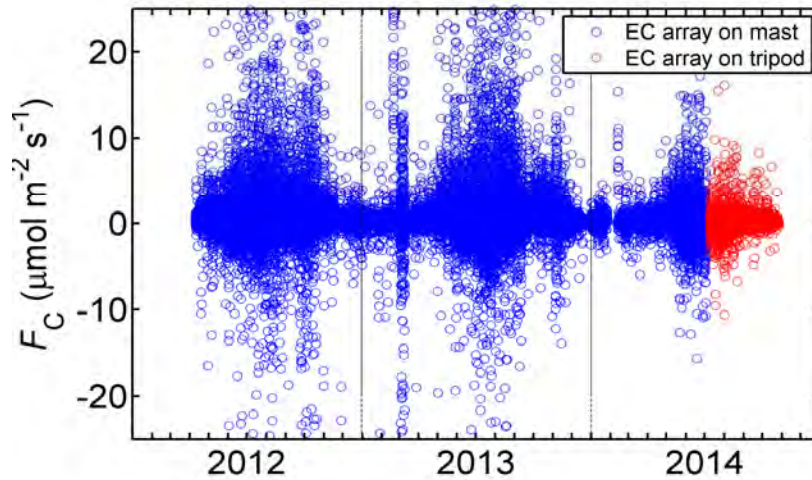


Figure 3.8: Half-hourly eddy-covariance measurements of CO<sub>2</sub> flux (FC) for May 2012 to October 2014 at pad 8-19. The EC sensors moved from the southwest quadrant to the southeast quadrant and lowered from the 2-m height to the 1-m height on 4 July 2014. (from the University of British Columbia / University of Victoria Eddy co-variance work)

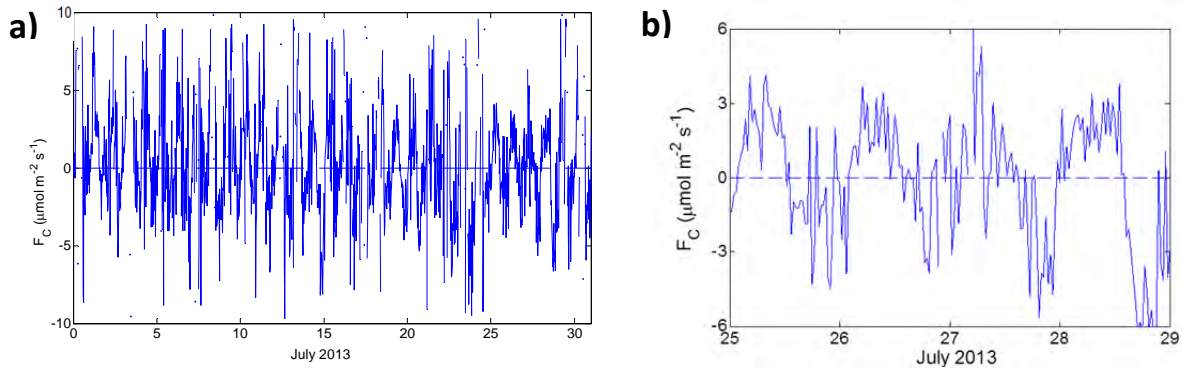


Figure 3.9: a) CO<sub>2</sub> fluxes measured by the eddy-covariance system mounted at the 2-m height on the post in the southwest sector of pad 8-19 in July 2013; b) Expanded view of the eddy-covariance CO<sub>2</sub> fluxes for July 25-29, 2013 showing strong negative daytime fluxes (photosynthesis) and strong positive nighttime fluxes (respiration). (from the University of British Columbia / University of Victoria Eddy co-variance work)

The CO<sub>2</sub> surface flux chamber data from July 2014 recorded by the Picarro and LiCOR systems ranged from about 0.3 to 6.5  $\mu\text{mol m}^{-2} \text{s}^{-1}$  at 5-35, and 0 to 5.0  $\mu\text{mol m}^{-2} \text{s}^{-1}$  at 8-19, depending on the lateral separation distance from the injection well and the instrument used for analysis (Fig. 3.10).

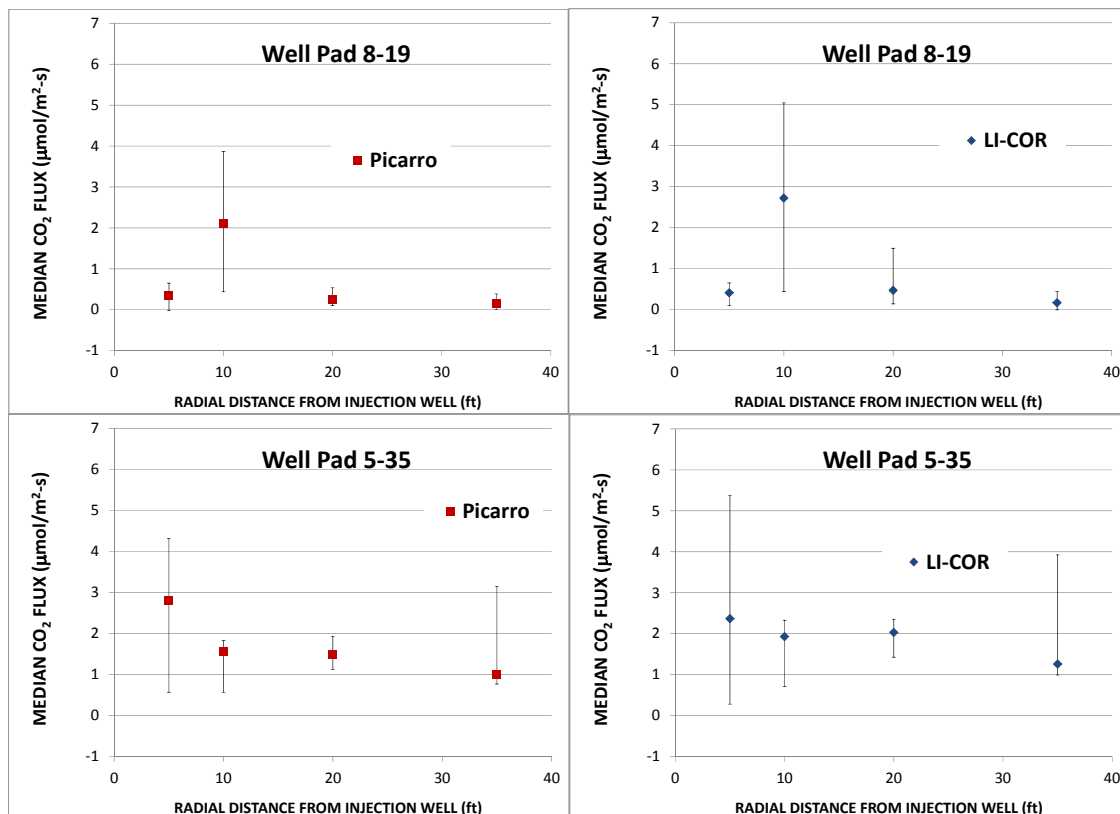


Figure 3.10: Median CO<sub>2</sub> fluxes ( $\mu\text{mol m}^{-2} \text{s}^{-1}$ ) as a function of radial distance from injection well at Well Pad 5-35 and 8-19 measured using the a) Picarro CRDS and b) LI-COR IRGA. Nb: extend of vertical black lines crossing median values represent min and max flux values recorded. (after Shell Projects and Technology (P&T) Soil and Groundwater and BioDomain teams)

At 5-35, a general increase in CO<sub>2</sub> fluxes can be observed as one moves closer to the injection well (Fig. 3.10). This is the case for both the median values determined for the Picarro and LI-COR instruments, which were generally in agreement. Note that at 5-35, CH<sub>4</sub> is detected near the IW (data not shown); and hence, oxidation of CH<sub>4</sub> is the likely cause for the slightly higher CO<sub>2</sub> levels. At 8-19 (Fig. 3.10), CO<sub>2</sub> flux values were in general < 1 μmol m<sup>-2</sup> s<sup>-1</sup> with small differences between the minimum and maximum values (< 0.8 μmol m<sup>-2</sup> s<sup>-1</sup>). An exception were the data recorded at 10 ft (~3 m) away from the injection well, where CO<sub>2</sub> flux values were higher and more variable among the 4 sampling points. This was observed for both the Picarro and LI-COR instruments, which were generally in agreement. The CO<sub>2</sub> flux values at 10 ft (~ 3 m) from the injector ranged from 0.5 to 5.0 μmol m<sup>-2</sup> s<sup>-1</sup>.

The CO<sub>2</sub> flux values determined using the radial chamber configuration up to a distance of 35 ft (10.5 m) away from an injection well on pads 8-19 and 5-35 were low and similar to flux data determined from the EC dataset. When comparing the pad specific CO<sub>2</sub> flux value determined via the EC dataset, there is good agreement with the farthest 35 ft (10.5 m) radial chamber configuration dataset. The EC footprint analysis at 8-19 indicates that the EC determined specific pad CO<sub>2</sub> flux covers an area outside the area covered by the radial chamber configuration (Fig. 3.11). Even though no EC measurements have been made at pad 5-35, it can be assumed that the similar observations can be made at 5-35, which is located about 5-6 km NW of 8-19. Note that “on-pad” CO<sub>2</sub> fluxes are significantly less than “off-pad” CO<sub>2</sub> fluxes, which was expected, considered that top soil was removed on the pad and “off-pad” sampling sites are highly vegetated.

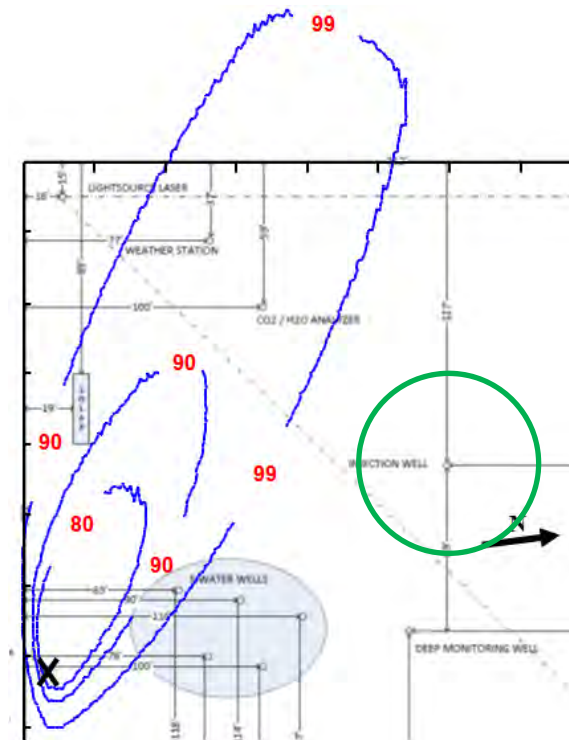


Figure 3.11: Daytime flux footprint (contours indicate % of flux footprint) determined for typical daytime values of climatic and site variables (e.g. wind speed, measurement height). Green circle indicates radial extend of the surface flux chambers setup discussed under section 2.3. Note that the nighttime flux footprint is similar (data not shown). (from the University of British Columbia / University of Victoria Eddy co-variance work)

As noted above, CO<sub>2</sub> flux measurements increase towards the injection well at 5-35. Corresponding median  $\delta^{13}\text{C-CO}_2$  values on the other hand showed a concomitant decrease (Fig. 3.12).  $\delta^{13}\text{C-CO}_2$  values ranged from -34.2 to -9.7 ‰, with about 94% of the data having a  $\delta^{13}\text{C-CO}_2 > -28$  ‰. These data fall within the range determined for  $\delta^{13}\text{C-CO}_2$  of above and below ground CO<sub>2</sub> (section 3.2), indicative of background atmospheric CO<sub>2</sub> and biological respiration associated with C3/C4 plants. The higher  $\delta^{13}\text{C-CO}_2$  values (~ -10 ‰) suggest possible short-circuiting of the flux chambers allowing above ground air entrainment into the chamber. The decrease in  $\delta^{13}\text{C-CO}_2$  values towards the injection well; however, suggest that another CO<sub>2</sub> source besides soil respiration / microbial degradation of old carbon (top soil was removed from pad) exists, as one would have expected the  $\delta^{13}\text{C-CO}_2$  values to be fairly uniform across the pad. The additional source being oxidation of CH<sub>4</sub>. The site conditions support this observation considering the presence of coal zones within 100 to 200 m below ground surface and the gas migration seen in the cellar of injection well 5-35. While CO<sub>2</sub> flux measurements did not indicate a consistent trend of increasing values towards the injection well at 8-19 (Fig. 3.10), the  $\delta^{13}\text{C-CO}_2$  values indicated a similar trend to the one observed at 5-35, with decreasing values towards the injection well

(Fig. 3.12).  $\delta^{13}\text{C-CO}_2$  values ranged from -78.2 to +48.1 ‰, and varied more compared to the data collected at pad 5-35.

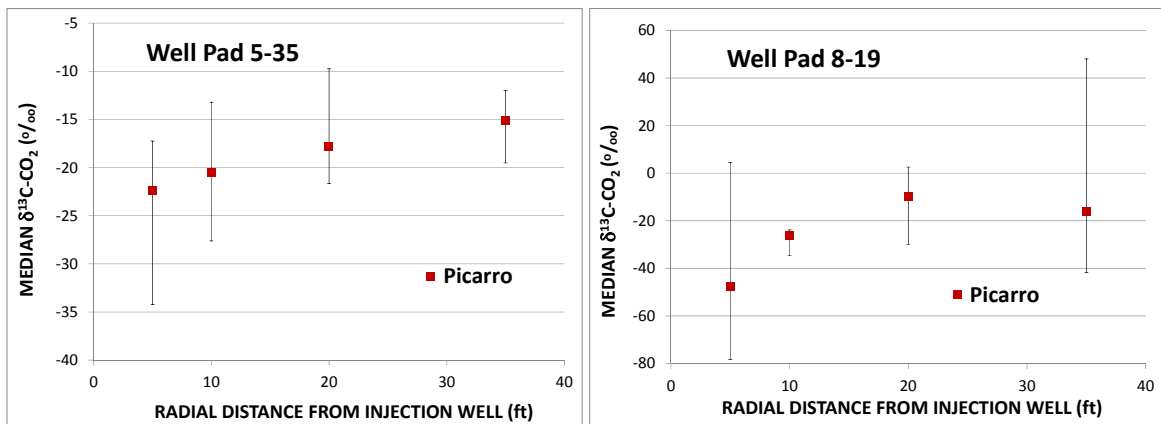


Figure 3.12: Median  $\delta^{13}\text{C-CO}_2$  values (‰) (determined using Keeling plot) as a function of radial distance from injection well at Well Pads 5-35 and 8-19 measured using the Picarro CRDS. Nb: extend of vertical black lines crossing median values represent min and max flux values. (from the Shell Projects and Technology (P&T) Soil and Groundwater and BioDomain teams)

### 3.2. Above ground atmosphere and soil gas data

Above ground atmosphere (ambient air)  $\text{CO}_2$  concentrations measured in the field using the GGA during the 2012-2014 HBMP activities ranged from 340 to 435 and 337 to 400 ppmv at 0.1 and 1 m elevation above ground surface, respectively (Fig. 3.13). Note that this range is based upon the mean  $\text{CO}_2$  concentration determined for each sampling point (idem elevation). Overall,  $\text{CO}_2$  concentration is slightly higher at 0.1 m elevation versus 1 m elevation, which can be expected considering closeness to the soil surface (the  $\text{CO}_2$  emitting source). The data also suggest the presence of a temporal trend in  $\text{CO}_2$  concentration in the ambient air.  $\text{CO}_2$  concentration at both 0.1 and 1 m elevation slightly increased from Winter to Fall to Spring; whereas in the Summer a decrease can be observed compared to the Spring values. This was observed in both 2013 and 2014 (data not shown) and is most likely related to increased photosynthetic activity over the summer months.

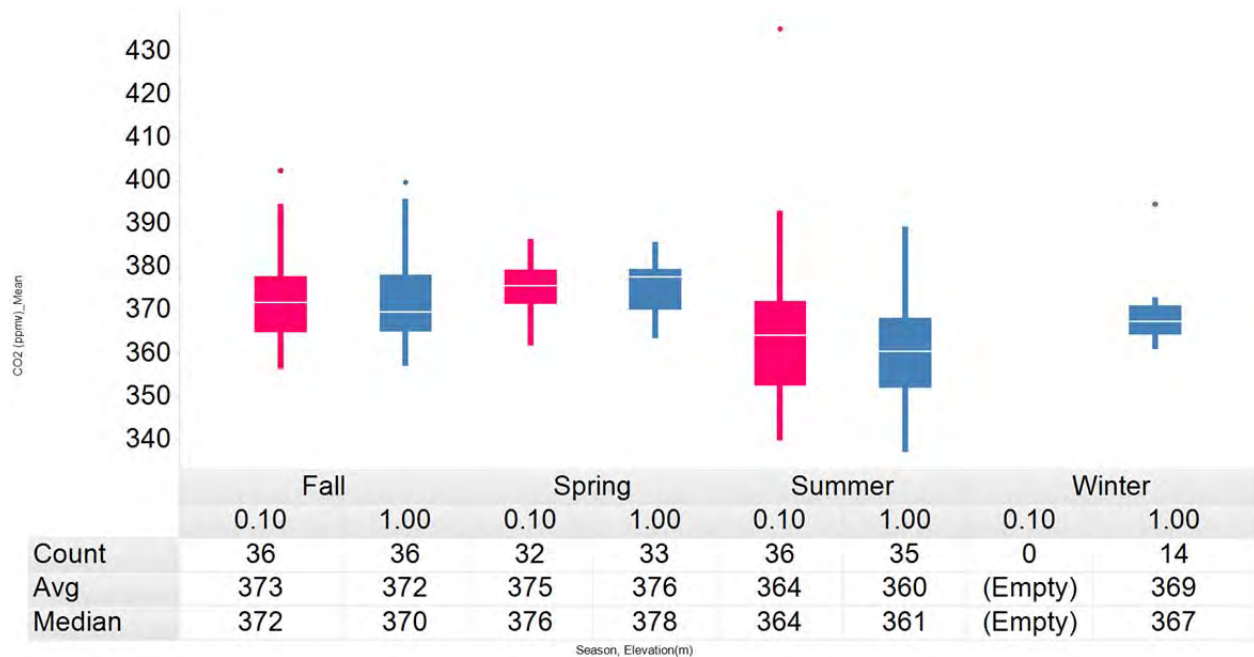


Figure 3.13: Box plot of ambient air CO<sub>2</sub> concentration (ppmv) at 0.1 (rose color) and 1 (blue color) m elevation by season for all data collected as part of the 2012-2014 HBMP sampling activities.

Spatially, CO<sub>2</sub> concentrations varied among land use types (Fig. 3.14). Forested areas (broadleaf (or deciduous) and coniferous) and pasture land use types tended to have slightly higher ambient CO<sub>2</sub> concentrations at both 0.1 and 1 m elevations above ground compared to other land use types. As well,

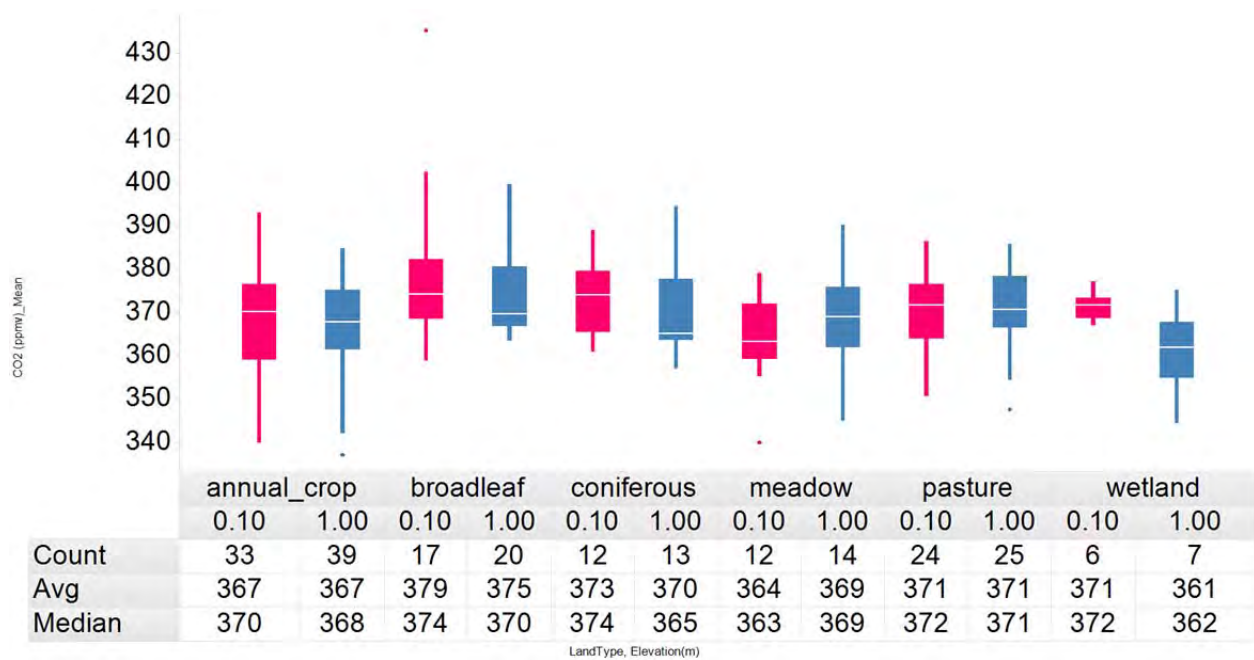


Figure 3.14: Box plot of ambient air CO<sub>2</sub> concentration (ppmv) at 0.1 (rose color) and 1 (blue color) m elevation by land use type for all data collected as part of the 2012-2014 HBMP sampling activities. Nb: broadleaf referred to as deciduous for box plots showing CO<sub>2</sub> flux data.



a difference in ambient CO<sub>2</sub> concentration was observed based on soil type (Fig. 3.15). Regosol had generally higher ambient CO<sub>2</sub> concentrations at both 0.1 and 1 m elevations above ground compared to other soil types.

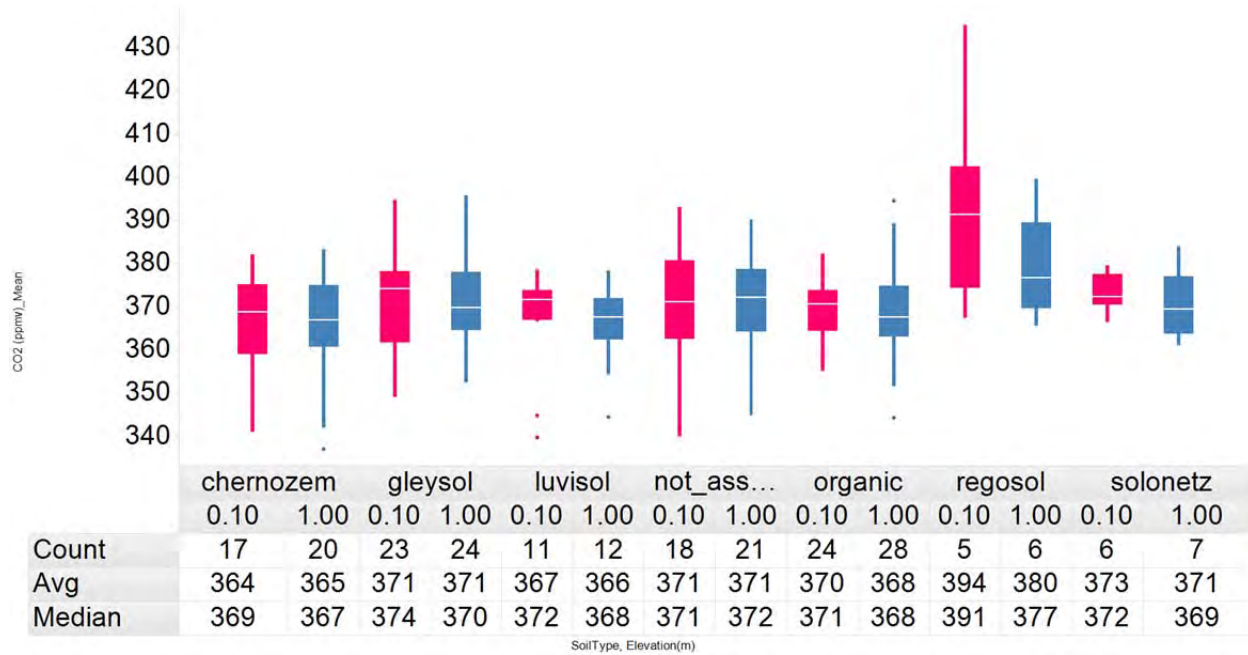


Figure 3.15: Box plot of ambient air CO<sub>2</sub> concentration (ppmv) at 0.1 (rose color) and 1 (blue color) m elevation by soil type for all data collected as part of the 2012-2014 HBMP sampling activities. Nb: broadleaf referred to as deciduous for box plots showing CO<sub>2</sub> flux data; for some sites, soil type is not available (referred to as not\_ass...).

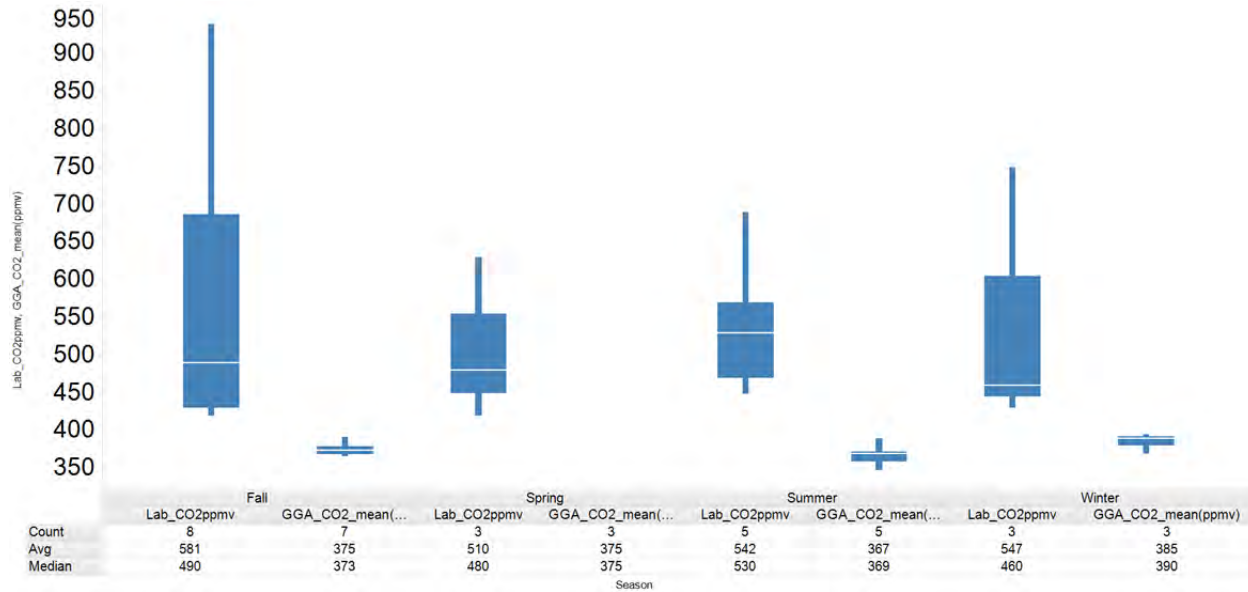


Figure 3.16: Box plot of ambient air CO<sub>2</sub> concentration (ppmv) at 1 m elevation by season for the discrete ambient air samples collected as part of the 2012-2014 HBMP sampling activities. Shown as well are the concomitant in-field measurements from the GGA instrument. Nb: (... refers to (ppmv)).

Besides the GGA in-field measurements, a number of discrete ambient air samples were collected at 1 m elevation above ground for laboratory analysis (Fig. 3.16). It is interesting to note that all laboratory samples have consistently higher CO<sub>2</sub> concentrations compared to the corresponding GGA measurements. For the discrete samples, δ<sup>13</sup>C-CO<sub>2</sub> values were also determined and ranged from -17.1 to -7.4‰, with an average value of -11.9±2.7‰. The low δ<sup>13</sup>C-CO<sub>2</sub> values suggest possible contamination with soil gas air (which may explain the higher CO<sub>2</sub> concentrations discussed previously) when considering the data that were obtained as part of the soil gas probe sampling of the 2012-2014 HBMP and the July 2014 in-situ field sampling campaigns, as discussed below.

For the latter, a limited number of the in-situ field measurements are available (at the time-of-writing this report) for soil gas and nearby above-ground atmosphere. At 8-19, CO<sub>2</sub> concentration for above-ground atmosphere (ambient air) was near 400 ppm; whereas, soil gas CO<sub>2</sub> concentration reached up to 1400 ppm. δ<sup>13</sup>C-CO<sub>2</sub> values changed concomitantly from around -10‰ for above-ground atmosphere to around -21.5‰ for soil gas. These δ<sup>13</sup>C-CO<sub>2</sub> values are typical for what is expected for ambient air and C3 vegetation (respiration / microbial degradation of soil organic matter). The δ<sup>13</sup>C-CO<sub>2</sub> values are also in agreement with the “off-pad” in-situ flux chamber measurements undertaken at 8-19 using the combined LiCOR - Picarro setup (see section 3.1.1).

The soil gas concentrations and δ<sup>13</sup>C-CO<sub>2</sub> values determined at the 8-19 site in July 2014 with the Picarro analyzer are in agreement with the soil gas data collected as part of the 2012-2014 HBMP sampling activities. For the latter, soil gas CO<sub>2</sub> concentrations ranged from 879 to 118450 ppmv and 500 to 71600 ppmv based on GGA in-field analysis and laboratory analysis, respectively (Fig. 3.17). Overall, there was good agreement between the GGA and laboratory analyses, except for some outliers primarily from the Spring and Summer 2014 datasets. With regards to the seasonal changes, soil gas CO<sub>2</sub> concentrations were in general highest in the Summer and lowest in the Winter compared to the other seasons, as would be expected based on biological activity (Fig. 3.18). Spatially, no clear trend was observed in soil gas CO<sub>2</sub> concentration between different land use types; however, soil gas CO<sub>2</sub> concentrations differed among soil types. Luvisol tended to have the highest soil gas CO<sub>2</sub> concentrations (Fig. 3.19). δ<sup>13</sup>C-CO<sub>2</sub> values ranged from -29.3 to -10.6‰. On a temporal basis, δ<sup>13</sup>C-CO<sub>2</sub> values tended to be highest in the Winter compared to the other seasons (Fig. 3.20). With regards to land use type, δ<sup>13</sup>C-CO<sub>2</sub> values tended to be highest for coniferous compared to the other land use types (Fig. 3.21); however, not clear



difference was observed between soil types. And on average,  $\delta^{13}\text{C-CO}_2$  values were similar between sampling depths of the soil gas probes.

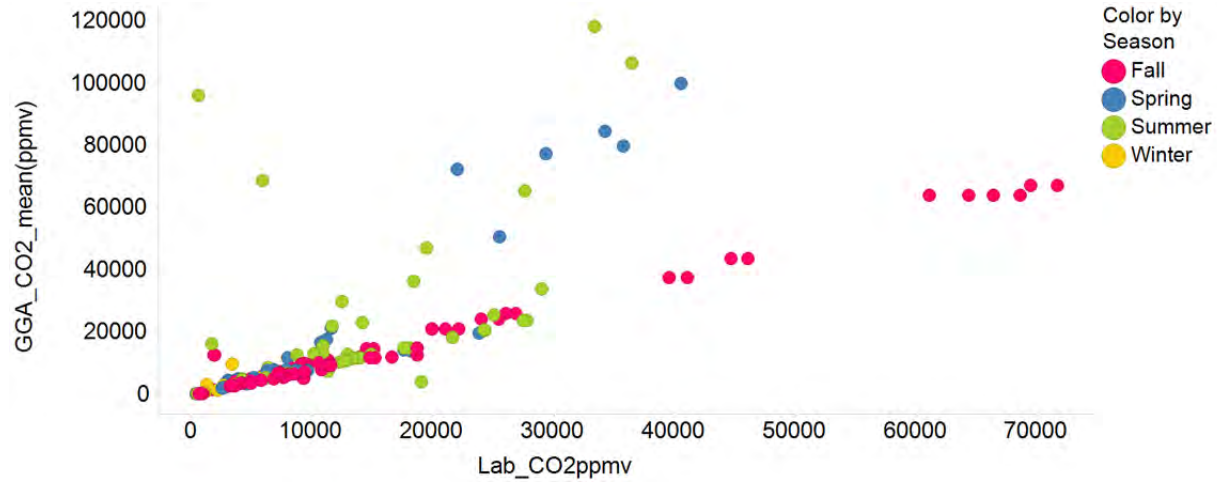


Figure 3.17: Cross-plot of soil gas CO<sub>2</sub> concentration (ppmv) measured by the GGA versus CO<sub>2</sub> concentration measured in the laboratory (ppmv) for all data collected as part of the 2012-2014 HBMP sampling activities.

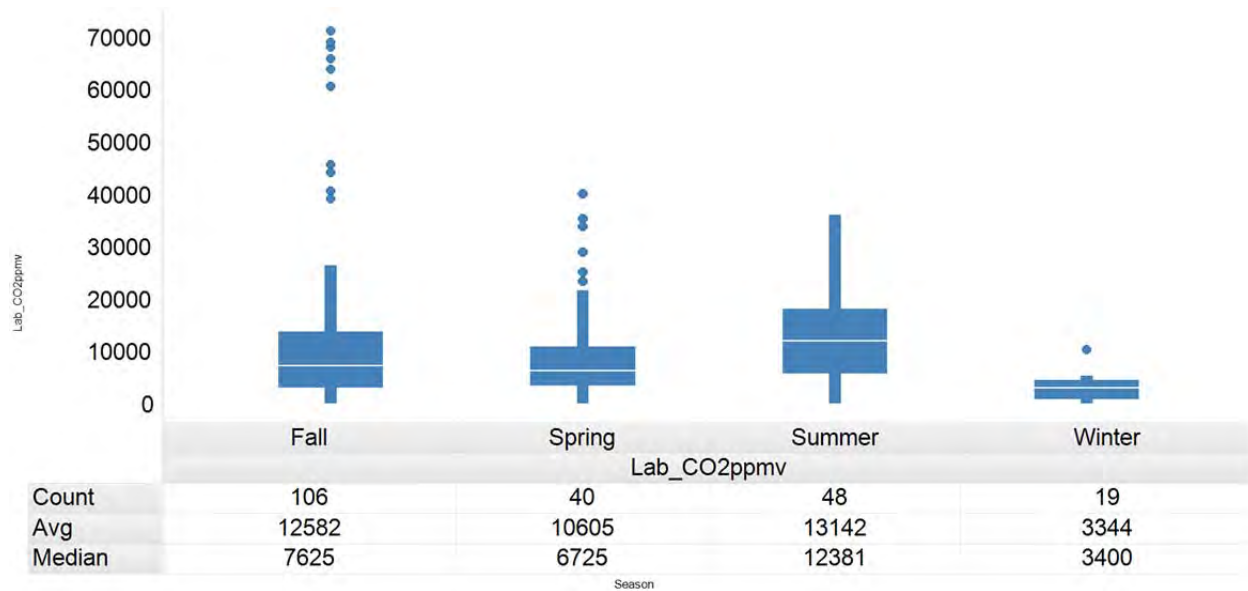


Figure 3.18: Box plot of soil gas CO<sub>2</sub> concentration (ppmv) by season for all samples collected as part of the 2012-2014 HBMP sampling activities.

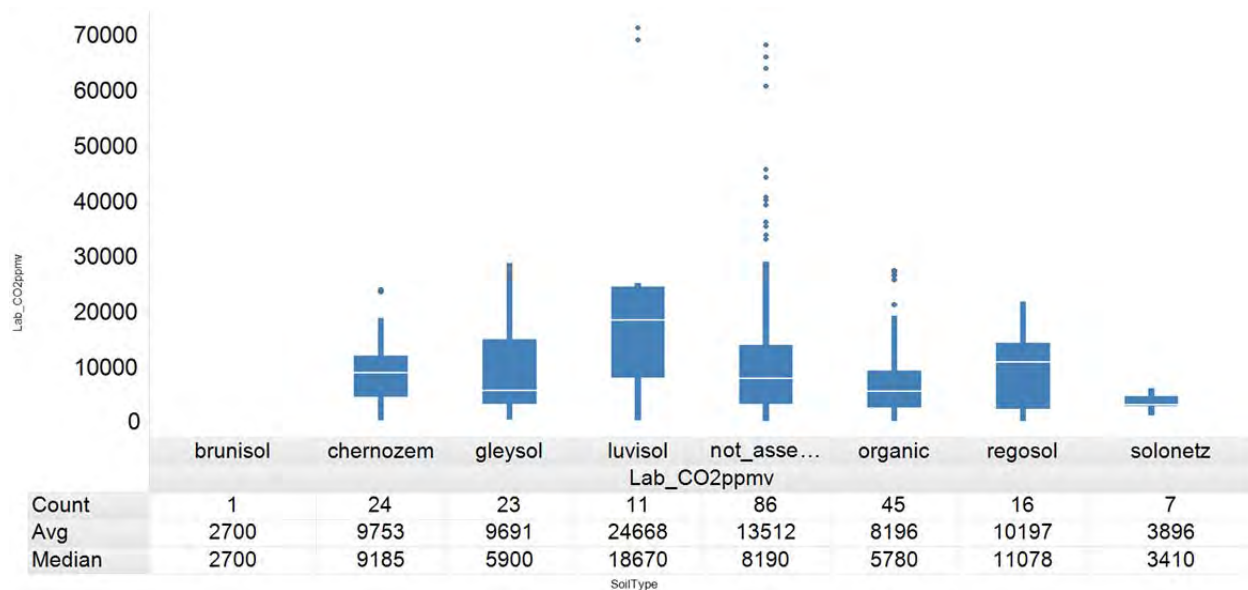


Figure 3.19: Box plot of soil gas CO<sub>2</sub> concentration (ppmv) by soil type for all samples collected as part of the 2012-2014 HBMP sampling activities. Note that for some sites, soil type is not available (referred to as not\_asse...).

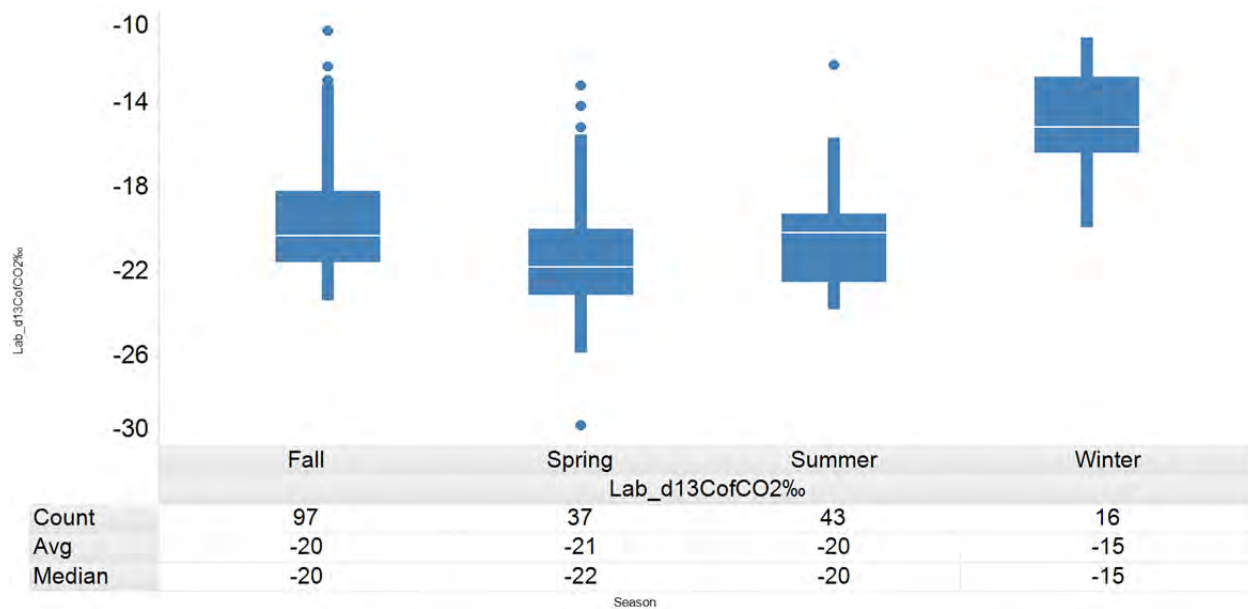


Figure 3.20: Box plot of soil gas δ<sup>13</sup>C- CO<sub>2</sub> values (‰) by season for all samples collected as part of the 2012-2014 HBMP sampling activities.

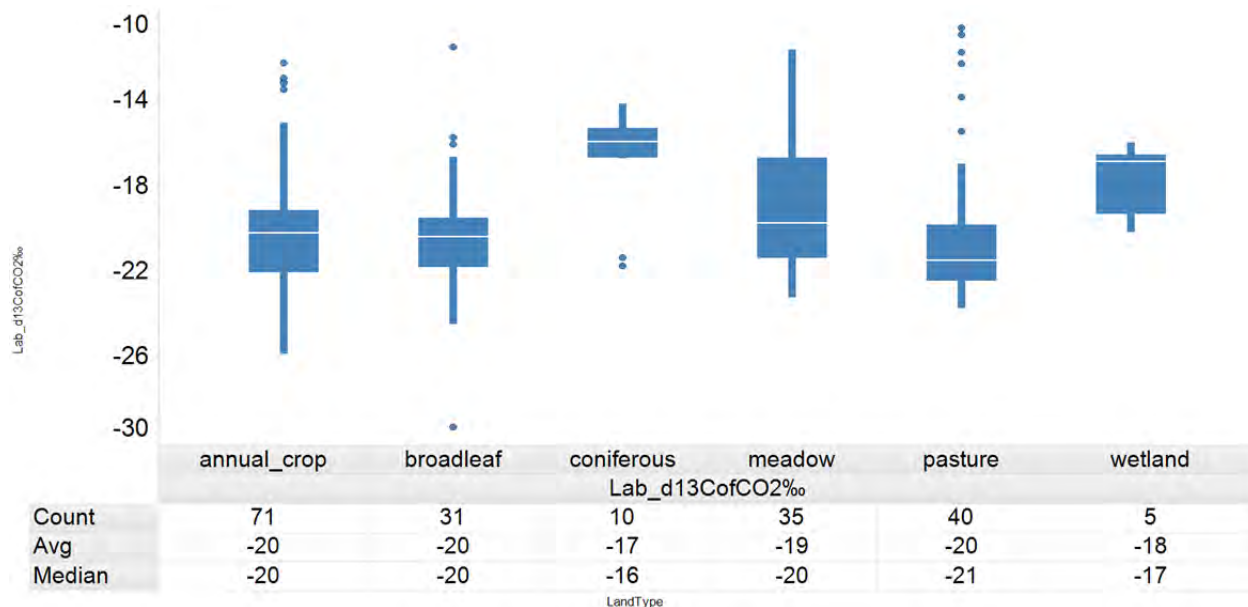


Figure 3.21: Box plot of soil gas  $\delta^{13}\text{C}-\text{CO}_2$  values (‰) by land use type for all samples collected as part of the 2012-2014 HBMP sampling activities.

### 3.3. CO<sub>2</sub> walk-over survey data

The walk-over survey at pad 5-35 yielded CO<sub>2</sub> concentrations near ambient (367 to 380 ppm) throughout the surveyed area (Fig. 3.22). As well, there was no consistent pattern observed in the  $\delta^{13}\text{C}-\text{CO}_2$  values throughout the surveyed area.  $\delta^{13}\text{C}-\text{CO}_2$  values were similar to expected  $\delta^{13}\text{C}$  of ambient air. The CO<sub>2</sub> data indicated little variation, and no distinct “plume” is evident above background. Similarly at pad 8-19, CO<sub>2</sub> concentrations were near ambient (Fig. 3.23). And, the  $\delta^{13}\text{C}-\text{CO}_2$  values were also fairly uniform across the surveyed area, with no distinct spatial pattern in the distribution of  $\delta^{13}\text{C}-\text{CO}_2$  values. At pad 7-11, CO<sub>2</sub> concentration were also near ambient throughout the surveyed area (Fig. 3.24). There appears, however, to be a slight spatial clustering in  $\delta^{13}\text{C}-\text{CO}_2$  values, with lower values corresponding to areas with higher CH<sub>4</sub> concentration (data not shown). No clear distinct CO<sub>2</sub> plume was evident above background data at pad 7-11, as was the case at 5-35 and 8-19.

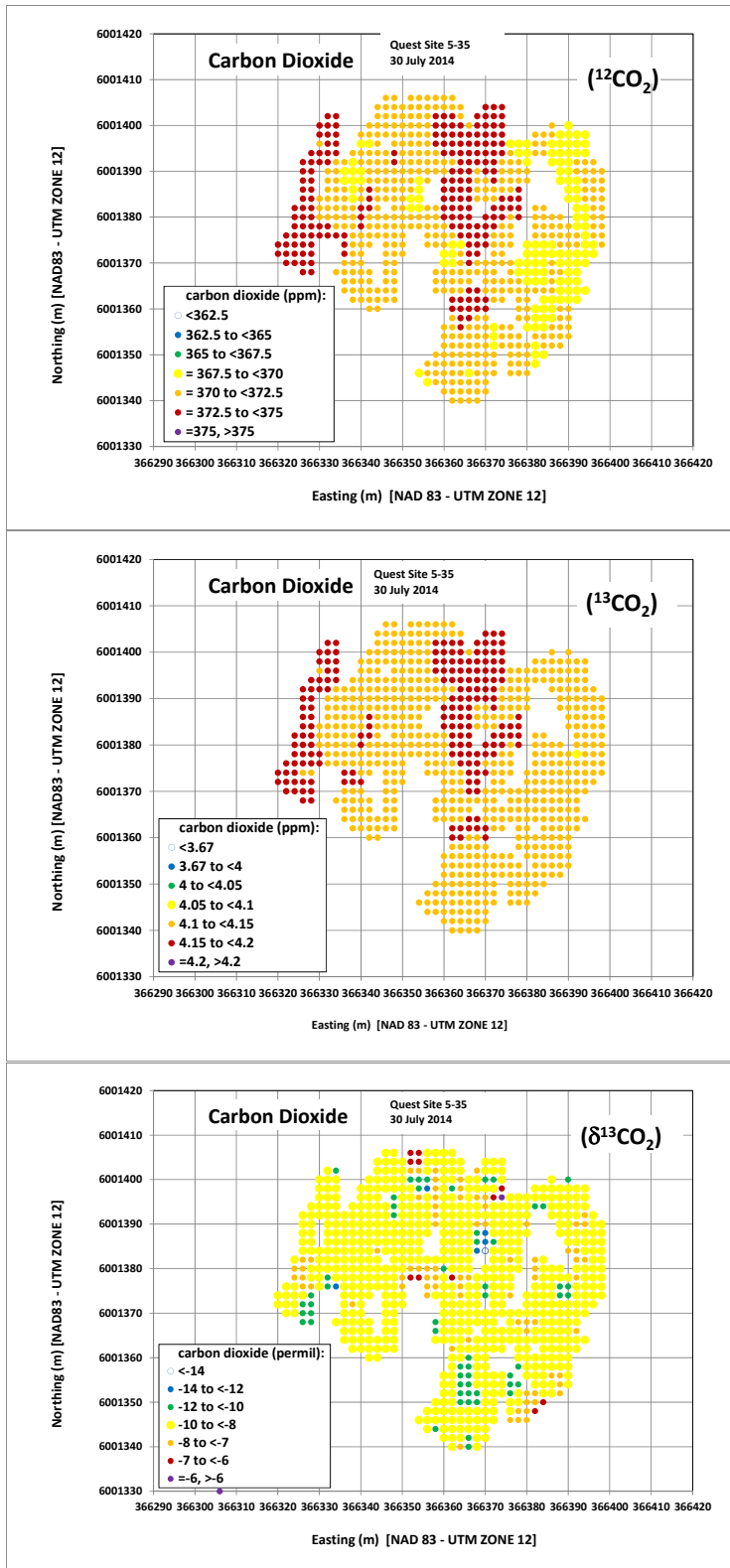


Figure 3.22: Spatial plots of air data mapped to regular grid for Well Pad 5-35. (from the Shell Projects and Technology (P&T) Soil and Groundwater and BioDomain teams)

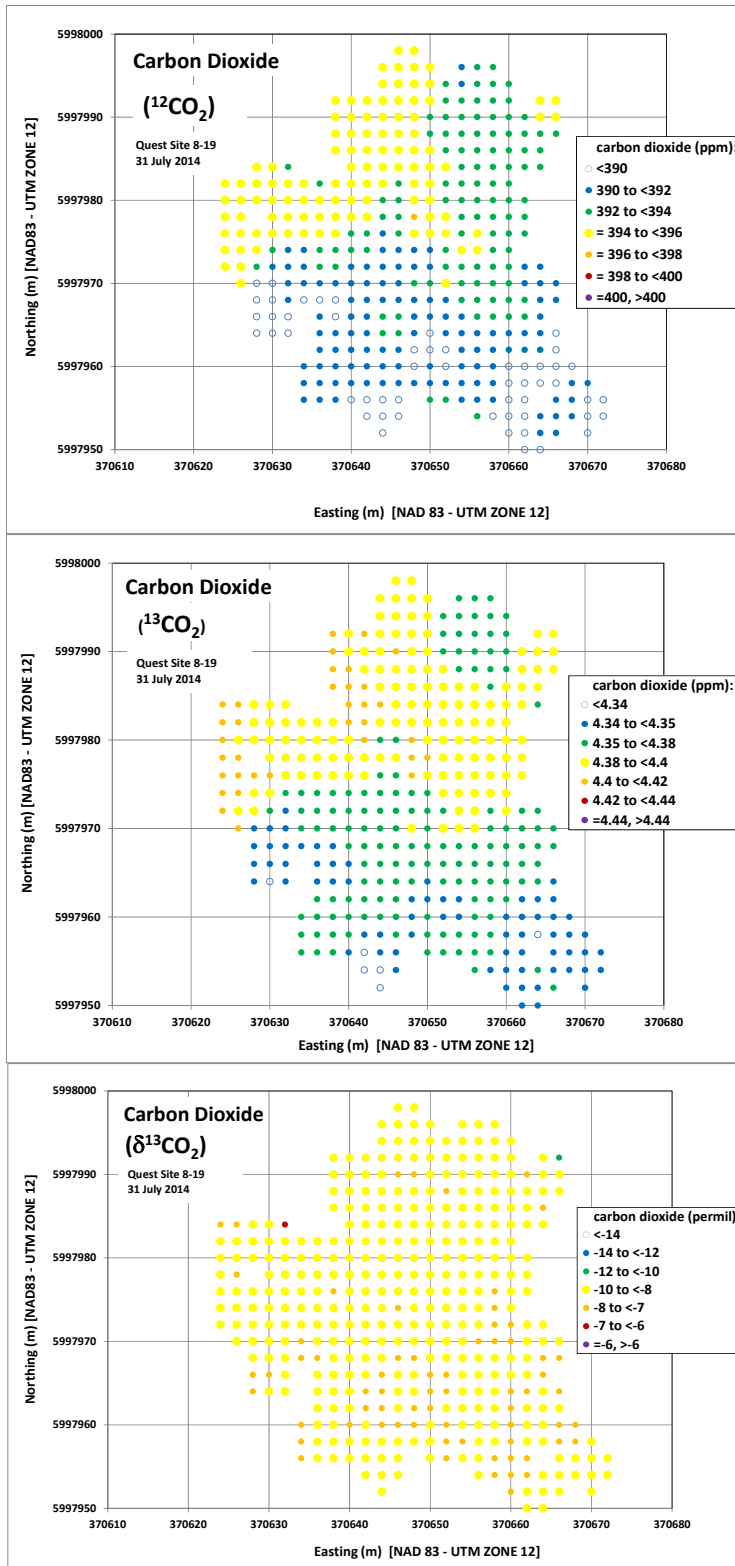


Figure 3.23: Spatial plots of air data mapped to regular grid for Well Pad 8-19. (from the Shell Projects and Technology (P&T) Soil and Groundwater and BioDomain teams)

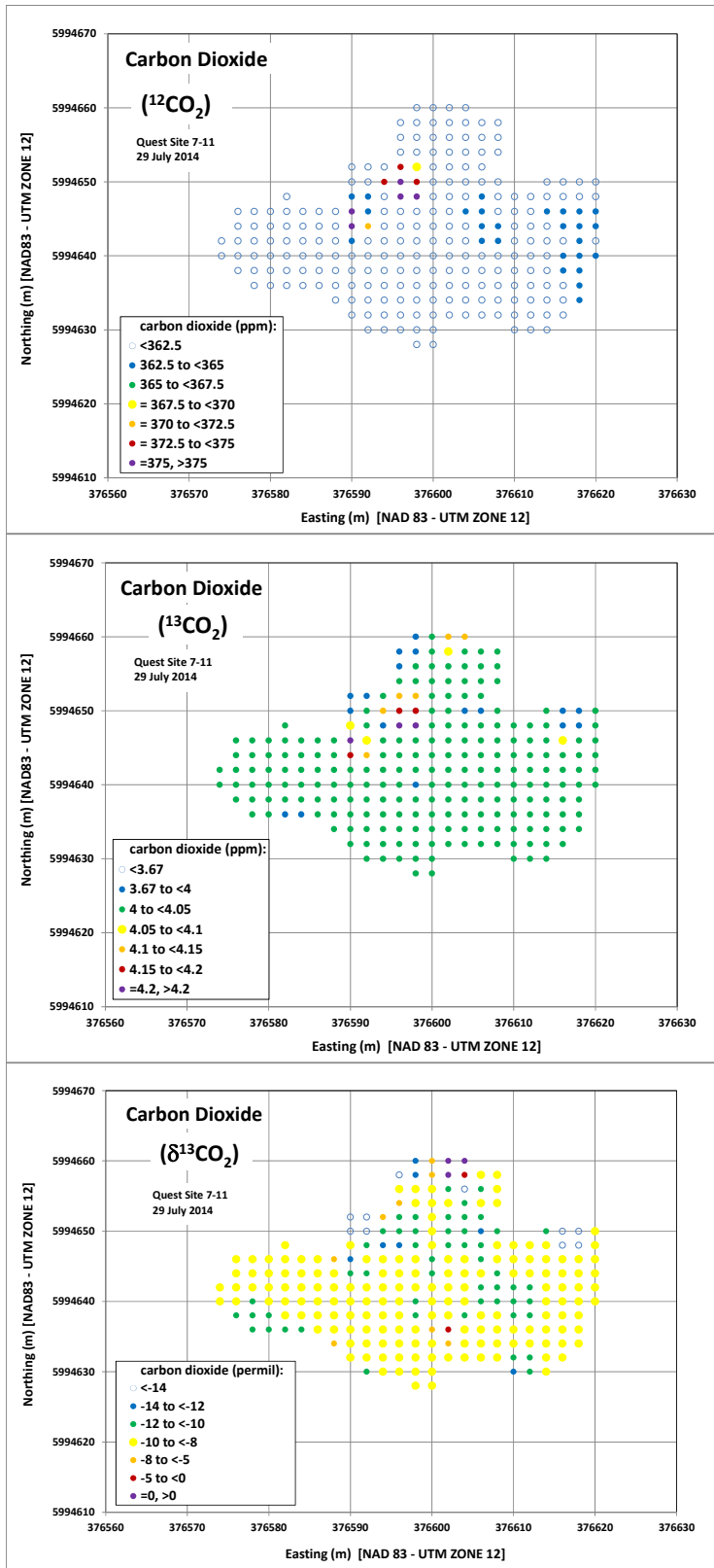


Figure 3.24: Spatial plots of air data mapped to regular grid for Well Pad 7-11. (from the Shell Projects and Technology (P&T) Soil and Groundwater and BioDomain teams)

## 4. Synopsis

An extensive and comprehensive dataset has been compiled with regards to soil surface CO<sub>2</sub> flux, ambient air and soil gas CO<sub>2</sub> concentration and isotopic composition across the Quest sequestration lease area. The various datasets were generally in agreement. Surface CO<sub>2</sub> fluxes ranged from <0.3 to >20 μmol m<sup>-2</sup> s<sup>-1</sup> on the injection well pads where the top soil has been removed and vegetated - highly biological active areas (e.g. cropland), respectively. Seasonal and spatial difference among the various datasets were assessed. The latter covering different the key land use and soil types within the Quest sequestration lease area.

## 5. Acknowledgements

Many thanks go to C. McNaughton and D. Coffen from Golder Associates Ltd; T.A. Black, N.J. Grant, Z. Nestic, R.S. Jassal, and H. Jones from the University of British Columbia; M.J. Whiticar from the University of Victoria; and M. Lahvis, C.A. Davies, G. DeVaul, and J. Guelfo from the Shell Projects and Technology (P&T) Houston Soil and Groundwater and BioDomain teams for their work related to this report.

APPENDIX E: SAR FEASIBILITY UPDATE



## Quest Brine Monitoring Baseline Work Summary

Cara Schiek-Stewart (SIEP-PTI/EB), James Sokolowski (Frontier Imaging Solutions), and Ed Biegert (SIEP-PTI/EB)

### Summary

Analysis of ground measurements and satellite imagery collected in the Quest area in 2012-2014 indicate that it is not feasible to derive soil moisture and conductivity directly from SAR satellite data alone and hence the radar imagery is not a viable candidate for direct detection of brine leakage.

Time-lapse morphological analysis of soil moisture patterns derived from SAR and optical satellite imagery using conventional analysis techniques provide an alternative indirect indicator of brine leakage.

This document is a summary of the work completed during the Baseline period. A full report will be generated at a later date, and all work provided here is available upon request.

### Field Campaigns

From 2012 to 2014, ground measurements and satellite imagery were collected in the Quest area for establishing a background environmental baseline as well as testing whether brine leakage can accurately be detected and monitored using satellite radar data. After some initial setbacks pertaining to the amount and techniques the samples were taken, we were able to test the proposed monitoring methodology using Synthetic Aperture Radar (SAR) to areally monitor for brine leakage during the period from fall 2013 to fall 2014. The datasets used in the study include 4 ground sampling programs (fall 2013, spring 2014, summer 2014, and fall 2014) along with associated radar and optical satellite imagery collected during the same temporal period. EM38 conductivity measurements were taken in the field during the complete baseline period, 2012-2014. The conductivity measurements covered the entire monitoring area. Survey data of roads and other infrastructure within the Quest area were used to determine the spatial accuracy of the satellite datasets as well as to improve it around ground sampling sites to ensure precise ground to satellite location sampling. In addition to the EM38 field measurements, soil moisture (water % on weight basis) and electrical conductivity (dS/m at 25 C) were measured in the laboratory from samples collected in the field during the fall 2013 and 2014 sampling campaigns. Approximately 10 soil samples were taken from each monitoring area. These laboratory measurements are direct comparisons to the SAR data since they are collected at the SAR penetration depth, 5 cm. The EM38 measurements (0.75 m depth) penetrated the soil much deeper than the SAR backscatter making comparisons between these datasets more difficult.

## SAR Imagery

The SAR signal is a complex image composed of two parts, amplitude and phase (or real and imaginary components). These components can provide information about surface properties such as moisture, conductivity, roughness (the smoothness of the surface), and, given temporal spans, ground deformation. SAR data are well-known for monitoring ground deformation (Burgmann et al., 2000), ice movement and growth (Dierking, 2013), and soil moisture (Kornelsen and Coulibaly, 2013). In particular, the amplitude portion of the radar image contains information about moisture and conductivity (Shao et al., 2003; Lanse et al., 2008). In this study, we tested the ability to calculate and monitor soil conductivity using estimates of the dielectric properties derived from the SAR data.

### Direct Brine Detection: Estimating Soil Moisture and Conductivity from SAR Data

Because of the interest in soil conductivity to detect brine, we conducted an experiment to resolve if soil conductivity could be estimated from SAR data alone. Comparison of the EM38 data from the fall 2012 campaign (deep conductivities) with the SAR amplitude evinced clustering: specifically two separate trends, a vegetation trend and another aligned with the soil conductivity properties (Figure 1).

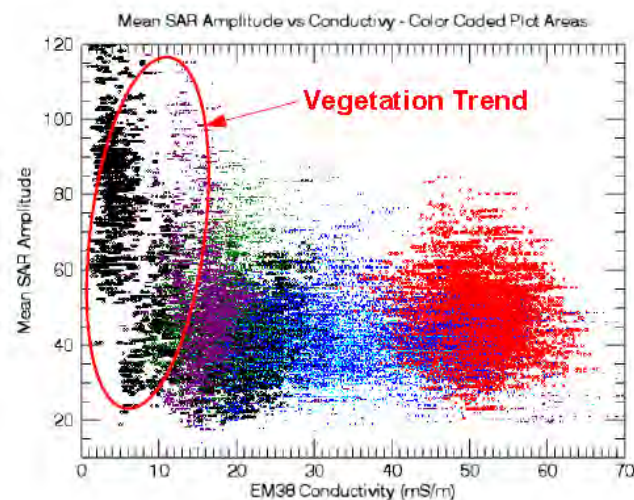
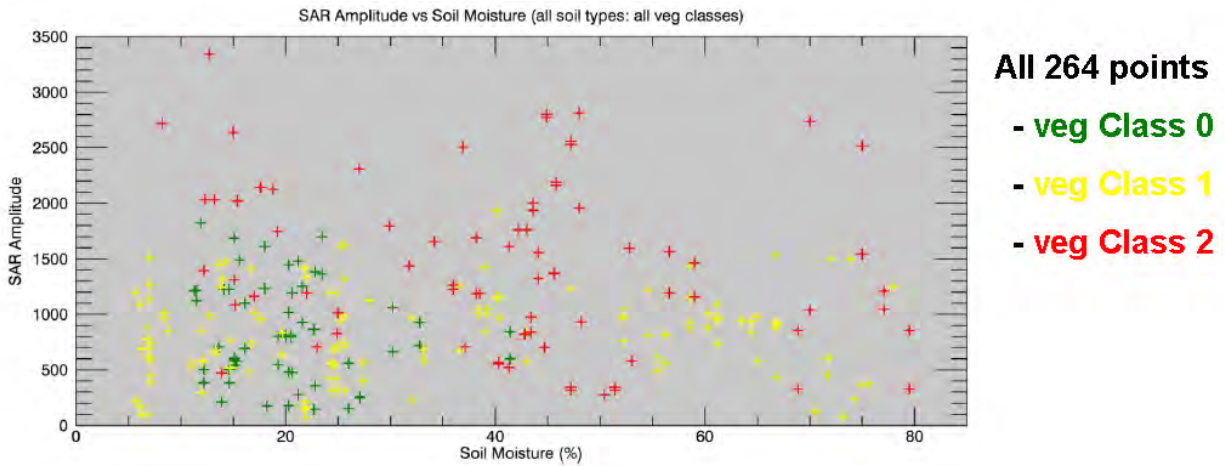


**Figure 1: Plot of SAR Amplitude vs. EM38 Conductivity. Colors denote Tier 1 subareas, areas with the highest spatial accuracy. Potential small positive correlation between SAR and EM38 by increased SAR amplitude with increased EM38 conductivity**

These initial results gave confidence in finding a correlation between soil conductivity versus SAR amplitude. Using the fall 2013 ground sampling dataset, we analyzed the data for trends. Each datum was classified into one of several vegetation classes (0= bare soil; 1 = grasses; 2 = forest) in order to distinguish among possible effects in the analysis due to ground cover. Figure 2 shows the initial results from the fall 2013 analysis.

A. SAR Amplitude vs Soil moisture for all vegetation classes



B. Soil Moisture (and Conductivity) vs SAR Amplitude for Vegetation Class 0 (Bare Soil) and 1 (Grasses)

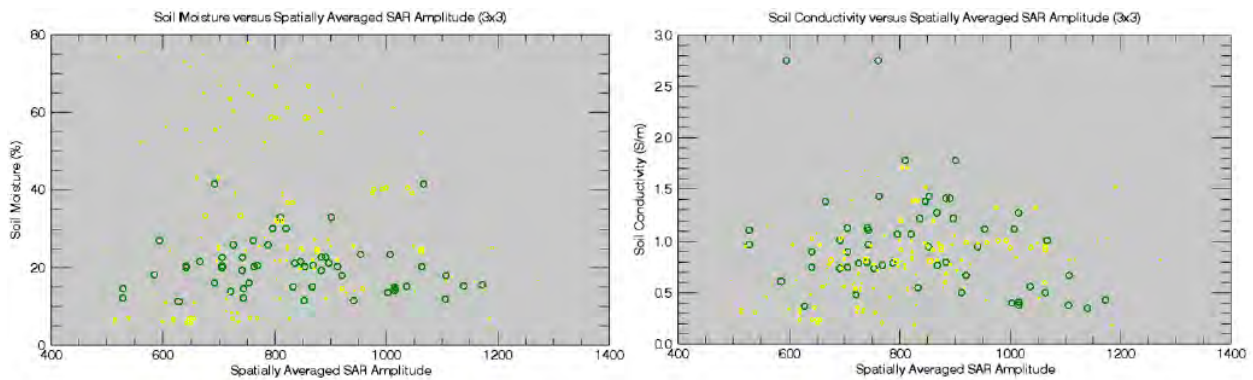
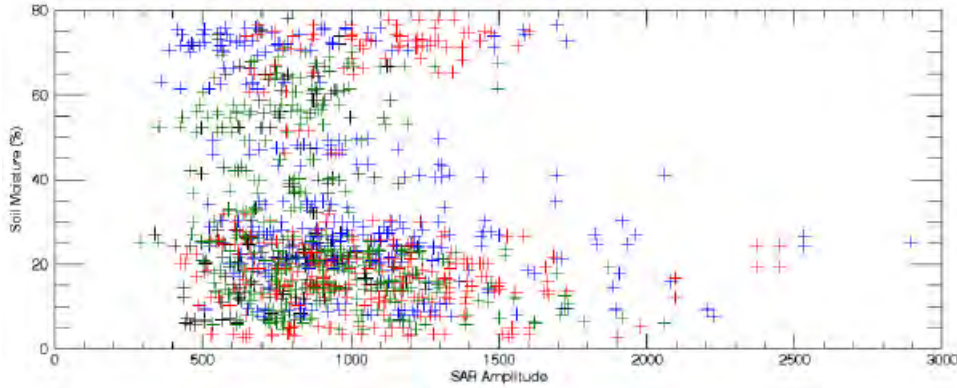


**Figure 2: Plots show the fall 2013 data analysis. Symbol color denotes vegetation class (Green: 0=bare soil, Yellow: 1=grasses, Red: 2=forest). Clusters and trends observed in the SAR vs. EM38 correlation are not evident in these data.**

The symbols in Figure 2 are color coded by vegetation (ground cover) and plotted as soil moisture and conductivity versus SAR amplitude from the fall 2013 campaign. Figure 2 illustrates two points: First, the vegetation trend observed in the prior analysis (Figure 1) was not replicated, and second, the data were too scattered, even when analyzed by vegetation class, to identify any reasonable correlation.

Once the 2014 field campaigns were completed, those data were added to the analysis (see Figure 3 below). These results indicate that it is not feasible to derive soil moisture and conductivity directly from SAR data alone.

- A. Soil Moisture vs. SAR Amplitude for vegetation class 0 (Bare Soil) and 1 (Grasses) covering fall 2013 (black), spring 2014 (blue), summer 2014 (red), and fall 2014 (green).



- B. Soil Conductivity vs. SAR Amplitude for vegetation class 0 (Bare Soil) and 1 (Grasses) covering fall 2013 (black), spring 2014 (blue), summer 2014 (red), and fall 2014 (green).

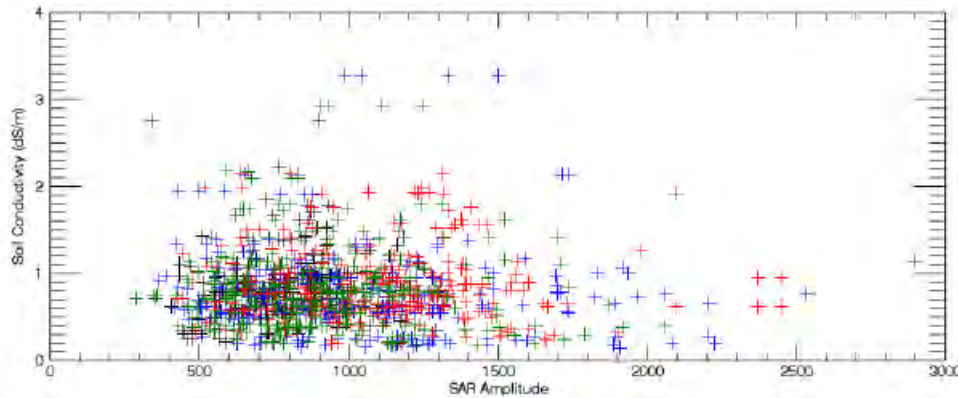


**Figure 3: Plots shows the multiple season calibration for data collected in years 2013 and 2014. Adding additional data did not improve the correlations or provide additional insight, thus leading the monitoring program into a new direction..**

Although these data indicate that it is not feasible to derive soil moisture and conductivity directly from SAR data alone, it may be possible to use SAR and/or optical satellite imagery as indirect indicators of brine leakage.

### **Indirect Brine Detection: Alternative Methodology**

Although it is not a direct indicator of brine leakage, soil moisture mapping is a standard product from MDA and other remote sensing service companies. These SAR-derived moisture maps are computed

using a different methodology that removes most of the incoherent noise in SAR prior to the moisture calculation. This differs from the procedure above, where none of the noise was removed. The soil moisture maps can be produced a number of different ways all of which approximate and remove noise in the SAR signal to achieve a more accurate spatial and temporal distribution of soil moisture (Kornelsen and Coulibaly, 2013). The current methods include using models to remove vegetation and backscatter effects prior to the computation. These models are based on either multiple datasets such as SAR, Optical, and Radiometrics (e.g. the Soil Moisture Active Passive (SMAP) Mission) or empirical relationships (Kornelsen and Coulibaly, 2013). Using this technology, the criterion for monitoring would be shape detection on the SAR-derived soil moisture map. During the conductivity exercise we observed that soil moisture anomalies mapped to anthropogenic activity (e.g. drainage and agriculture fields). By regularly examining these maps or examining them when a leak is thought to occur, the potential leak should have a morphology that does not fit the normal surface anthropogenic activity. This type of monitoring should be done prior to any other satellite monitoring using vegetation since vegetation can take longer to be affected by the leak. This new monitoring program only changes the SAR portion of the original program (Figure 4). This is updated in the figure below. The changes are highlighted by the underlined.

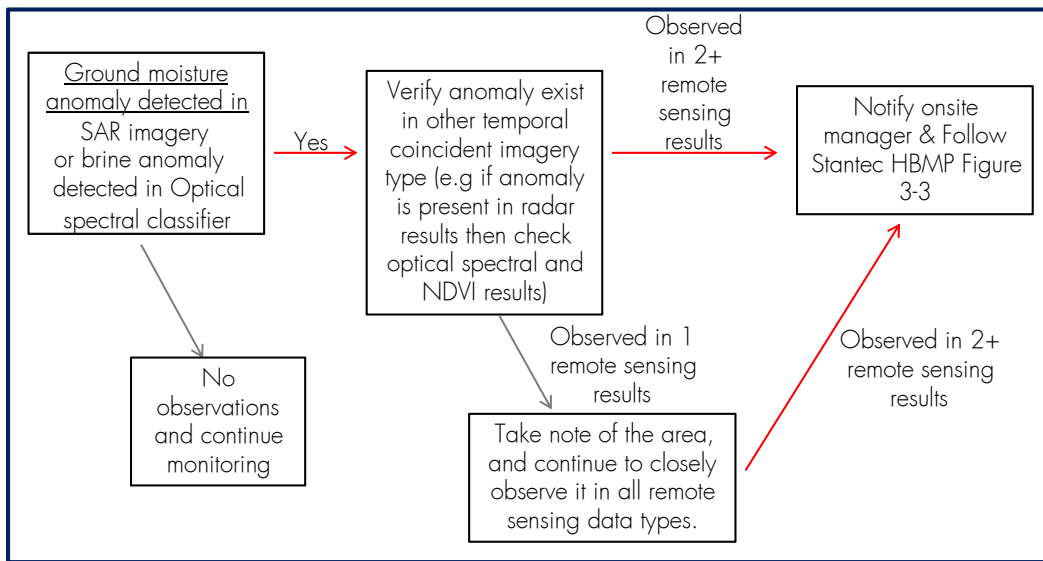


Figure 4: Modified anomaly verification decision tree taken from Schiek et al., 2012.

## REFERENCES

Burgmann, R.; Rosen, P.A.; Fielding, E.J. (2000), "Synthetic aperture radar interferometry to measure Earth's surface topography and its deformation", *Annual Review of Earth and Planetary Sciences* **28**: 169–209.

Dierking, W (2013), "Sea ice monitoring by synthetic aperture radar", *Oceanography* **26**(2):100–111, <http://dx.doi.org/10.5670/oceanog.2013.33>.

Kornelsen, K.C. and Coulibaly, P. (2013), "Advances in soil moisture retrieval from synthetic aperture radar and hydrological applications", *Journal of Hydrology* **476**: 460–489.

Lasne, Y., Paillou, P., Freeman, A., Farr, T., McDonald, K.C., Ruffles, G., Malezieux, J., Chapman, B., and Demontoux, F. (2008) "Effect of Salinity on the Dielectric Properties of Geological Materials: Implications for Soil Moisture Detection by Means of Radar Remote Sensing". *IEEE Trans. On Geosciences and Remote Sensing* **46**(6):1647-1688.

Schiek, C., Baker, R, and Biegert, E.K., (2012), "Remote Sensing Monitoring Plan for the Quest CO<sub>2</sub> Storage Site", Shell Internal Report SR.12.11355

Shao, Y., Hu, Q., Guo, H., Lu, Y., Dong, Q., and Han, C., (2003), "Effect of dielectric properties of moist salinized soils on backscattering coefficients extracted from RADARSAT image", *IEEE Trans. Geosci. Remote Sens.* **41**(8):1879–1888.

APPENDIX F: TRE REPORT ON INSAR DETECTION CAPABILITY

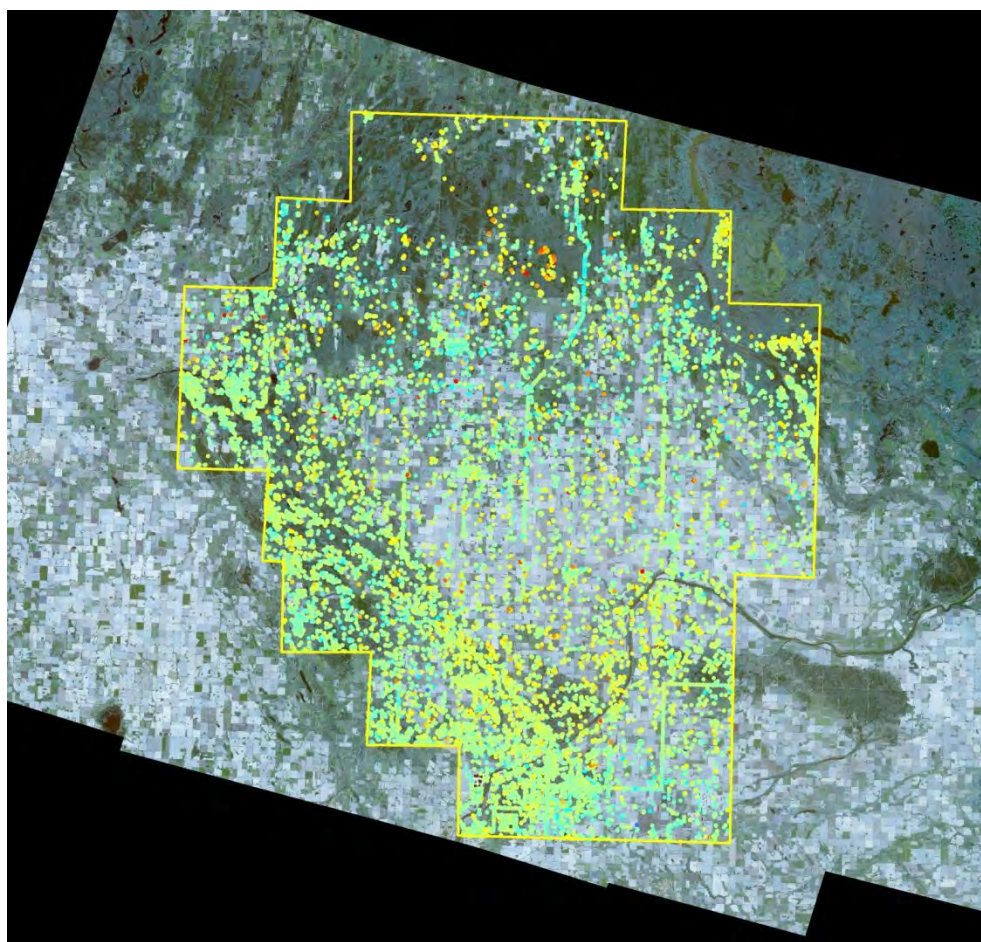




**TRE**<sup>®</sup>  
Sensing the Planet

# Monitoring Report

*2014 Update to Baseline Monitoring  
over the Quest Site*



Contract no. 4900019663

Submitted to:

Shell Canada Energy  
400 4th Avenue SW., P.O. Box 100 Station M,  
Calgary, AB  
T2P 3H7

Prepared by:

TRE Canada Inc.  
Doc. Ref.: JO14-3026-REP1.0

29 August 2014



## **Executive Summary**

TRE Canada Inc. has been contracted by Shell to perform a SqueeSAR analysis of the first three years of radar imagery collected over the Quest Carbon Capture and Storage injection site. Two sets of 45 images acquired between 03 June 2011 and 05 July 2014 with the Radarsat-2 satellite were processed with TRE's proprietary SqueeSAR™ algorithm. This report describes the results of the analysis.

The key findings are summarized below:

- Results indicate that minimal ground movement is occurring over the area analyzed. Deformation trends are consistent with the initial baseline analysis conducted over this area in December 2012.
- Mild fluctuations in many of the time series suggest seasonal variations of ground movement are present over much of the site.
- Measurement point density has increased from 10.6 to 14.5 points per square kilometre compared to the initial baseline analysis. This includes an average increase of 36% in the areas around the 3 injection wells.

The deliverables for this stage of the project include the present report and the displacement data.

## Table of Contents

1	Background.....	3
2	Overview of the Area of Interest .....	4
3	Radar Data.....	5
4	Data Processing .....	6
4.1	Large Area Processing Approach.....	6
4.2	Reference Point.....	7
5	Results of the SqueeSAR Analysis .....	8
5.1	Displacement Rate .....	8
5.2	Displacement Rate Standard Deviation .....	9
6	Observations .....	10
6.1	Injection Site.....	10
6.2	Comparison of Results.....	13
6.3	Target Distribution and Density around Injection Wells .....	15
6.3.1	Injector SCL 5-35 .....	16
6.3.2	Injector SCL 8-19 .....	18
6.3.3	Injector SCL 7-11 .....	20
7	Conclusions.....	22

## 1 Background

The Quest Carbon Capture and Storage Project will reduce emissions from Shell's Scotford Upgrader, located near Fort Saskatchewan, Alberta, by capturing, transporting, and storing over a million tonnes of CO<sub>2</sub> per year.

TRE Canada Inc. (TRE) has been contracted by Shell to provide an updated analysis of ground movement, building on an initial InSAR processing that was carried out over the Quest project site at the end of 2012. The present analysis utilized an additional 18 months of imagery in comparison to the first baseline analysis, covering from June 2011 to July 2014. The data processing was carried out using TRE's proprietary SqueeSAR™ algorithm coupled with imagery acquired by the Radarsat-2 satellite in Wide Multi-look Fine mode. This report describes the results of the analysis, including the density and distribution of scatterers identified over the AOI, and compares them to the initial baseline processing.

## 2 Overview of the Area of Interest

The Quest Project site is situated approximately 80 kilometres northeast of Edmonton, Alberta. The area of interest (AOI) as indicated by Shell has a total area of 3,750 km<sup>2</sup> (Figure 1). Few man-made structures are present at this site, with the exception of some small towns, roads and other infrastructure.

Agriculture is extensive throughout the central portion of the AOI while forested areas occupy much of the northern and western portions of the AOI. The area has a humid continental climate with a relatively high amount of annual precipitation and minimal topographic variation. Snow fall, which can limit radar reflectivity, is present for up to six months a year.

The injection well sites and pipeline that will transport the CO<sub>2</sub> from the Scotford Upgrader are shown in Figure 1. Note that all figures and images in this report use the North American Datum 1983 and the Universal Transverse Mercator zone 12N projection.

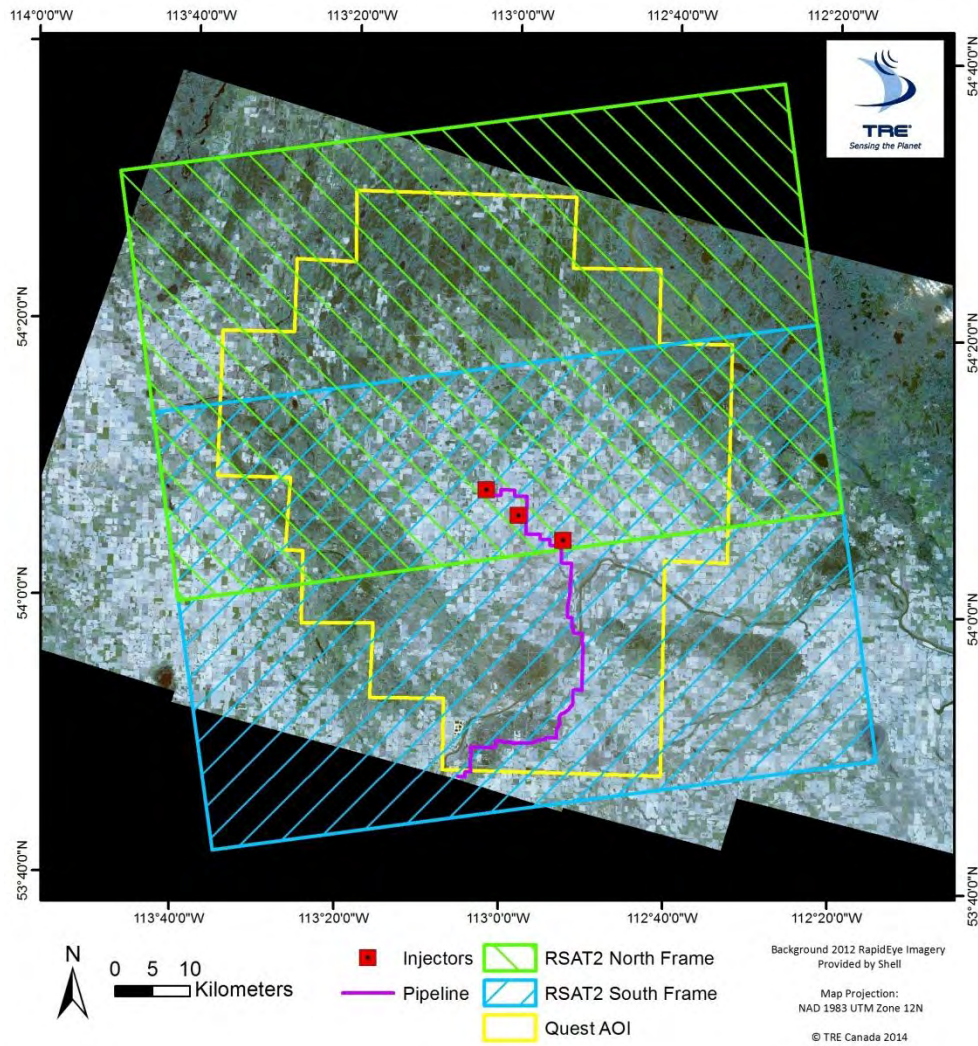


Figure 1: The Area of Interest (AOI) for the Quest project as indicated by Shell.

### 3 Radar Data

The imagery analyzed for this data processing was provided to TRE by Shell and consisted of 45 images acquired by the Radarsat-2 (RSAT-2) satellite (Table 1). Two RSAT-2 scenes are currently required for complete coverage of the Quest Project site (Figure 1). All images were acquired with a 24-day repeat interval using the Wide Multi-look Fine beam Mode 3 in an ascending orbit (meaning the satellite is travelling from south to north and imaging to the east) and cover a period of three years (mid-2011 to the mid-2014). One acquired image was discarded due to the presence of excessive atmospheric noise (highlighted in red in Table 1).

Number	Image dates	Number	Image dates
Initial Baseline Analysis		Updated Analysis	
1	06/03/2011	23	01/23/2013
2	06/27/2011	24	02/16/2013
3	07/21/2011	25	03/12/2013
4	08/14/2011	26	04/05/2013
5	09/07/2011	27	04/29/2013
6	10/01/2011	28	05/23/2013
7	10/25/2011	29	06/16/2013
8	11/18/2011	30	07/10/2013
9	12/12/2011	31	08/03/2013
10	01/05/2012	32	08/27/2013
11	01/29/2012	33	09/20/2013
12	02/22/2012	34	10/14/2013
13	04/10/2012	35	11/07/2013
14	05/04/2012	36	12/01/2013
15	05/28/2012	37	12/25/2013
16	06/21/2012	38	01/18/2014
17	07/15/2012	39	02/11/2014
	08/08/2012	40	03/07/2014
18	09/01/2012	41	03/31/2014
19	09/25/2012	42	04/24/2014
20	10/19/2012	43	05/18/2014
21	11/12/2012	44	06/11/2014
22	12/06/2012	45	07/05/2014

Table 1: Dates of the acquired Radarsat-2 images. The image highlighted in red was excluded from processing due to excessive atmospheric noise.

## **4 Data Processing**

### **4.1 Large Area Processing Approach**

Increases in computational capacities and experience with the area allowed the processing of the full scene for both image stacks (Figure 2). The data was then seamlessly integrated by cross-calibrating the results to ensure continuity throughout the entire AOI. In the previous data processing it had been necessary to divide the AOI into four distinct areas (tiles) and process each separately.



## 4.2 Reference Point

SqueeSAR is a differential technique, meaning displacement is measured compared to a stable reference point. Both image stacks have an individual reference point (Figure 2) which was selected using an optimization procedure which maximizes the quality of the results based on a suite of radar parameters including high coherence, low standard deviation values and low variability of movement over time.

Reference point coordinates for the current analysis are listed in the associated Appendix.

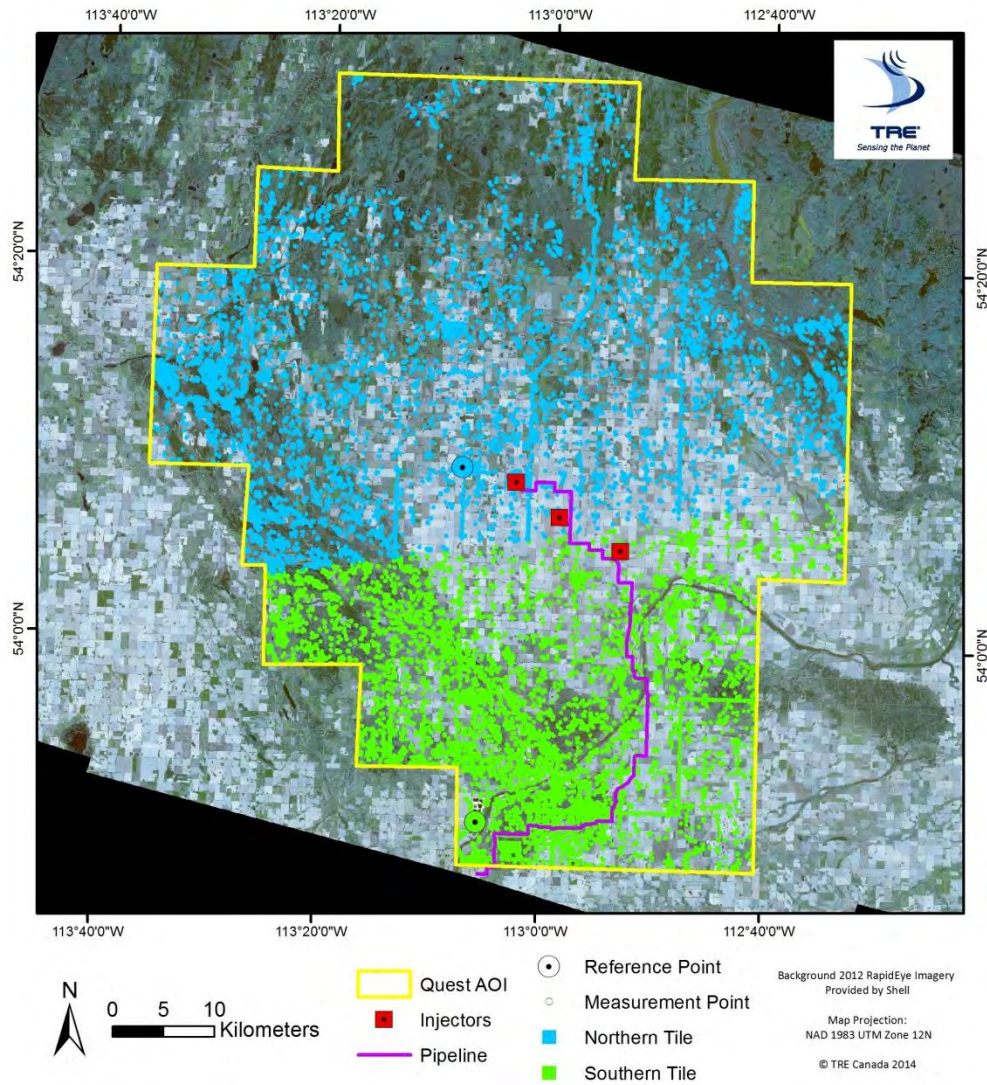


**Figure 2: Measurement points obtained from the processing of the two RSAT2 scenes along with their respective reference points. The reference point and all individual measurement points of both tiles are visualized using separate colors.**

## 5 Results of the SqueeSAR Analysis

### 5.1 Displacement Rate

The line-of-sight (LOS) displacement rates, expressed in both millimeters per year (mm/year) and inches per year (inches/year), are shown in Figure 3. Each point corresponds to a Permanent Scatterer (PS) or Distributed Scatterer (DS), and is color-coded according to its annual rate of movement. Average displacement values are calculated from a linear regression of the ground movement measured over the entire period covered by the satellite images, and should be interpreted taking into account their associated standard deviations (section 5.2). Detailed information on ground motion is also provided by means of displacement time series, which are provided for each PS and DS (Section 2).

Most of the AOI is relatively stable, with a measured average displacement rate of -0.22 mm/year, and no strong deformation patterns. Almost half of the measurement points identified have an annual displacement rate that is sub-millimetric, or within  $\pm 1$  mm/year.

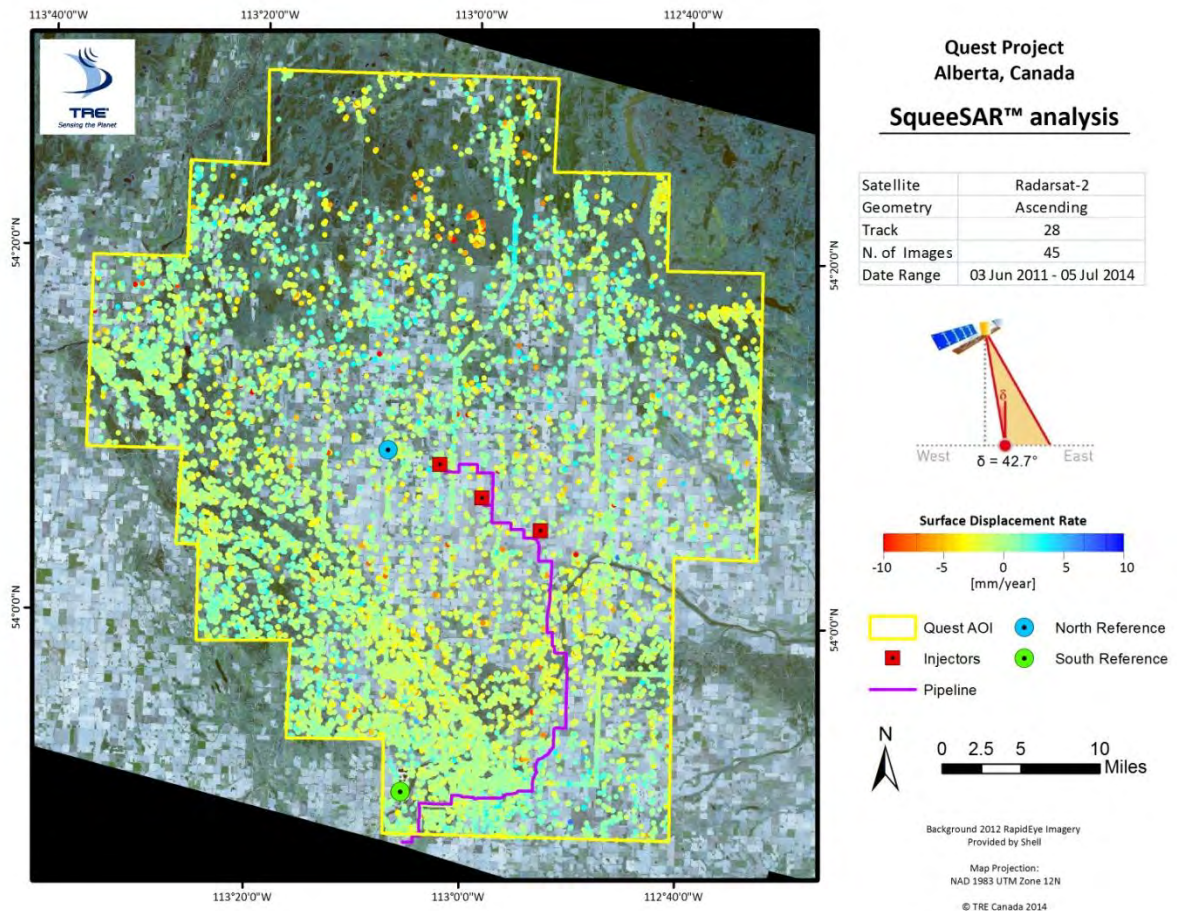


Figure 3: PS and DS deformation rates, expressed in mm/year.



## 5.2 Displacement Rate Standard Deviation

The standard deviation of the surface displacement data characterizes the error of the measurements (Figure 4). For this reason, any measurement should be interpreted in the form of Displacement Rate  $\pm$  Standard Deviation. Standard deviation values tend to increase with distance from the reference point. Higher values indicate a greater variability in displacement rates and are often associated with areas of rapid and/or irregular ground movement. As for displacement rates, standard deviation values are expressed in mm per year.

Standard deviation values are low throughout the AOI, ranging from 0.13 to 1.97 mm/year. Slightly higher standard deviation values were identified over areas with the strongest movement rates, particularly for points located furthest away from the reference points. The average standard deviation value of all measurement points within this data set is  $\pm 0.87$  mm/year.

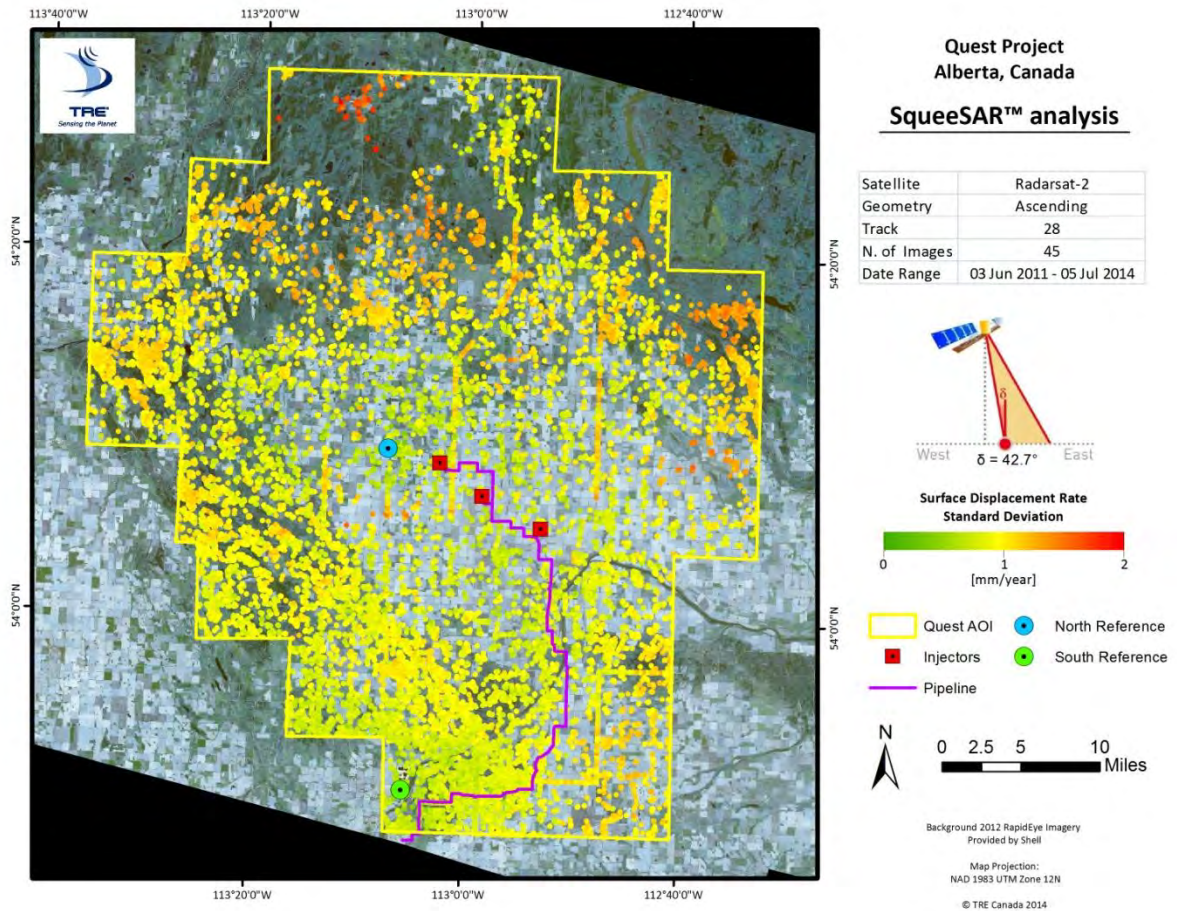


Figure 4: Standard deviation values of the displacement rates.

## 6 Observations

### 6.1 Injection Site

Measurement points identified in close proximity to the future site of injection indicate that the ground is relatively stable (Figure 5). Three wells have been drilled within the Quest AOI (Table 2). Average time series were created for all measurement points within a 1 km buffer of the three wells to examine any potential movement trends (Figure 6 to Figure 8, inclusive). Average time series are created by averaging the displacement measured by all points within a defined region.

Results indicate that no strong movement trends are present. Mild variations in surface displacement patterns are likely related to seasonal movement caused by freeze/thaw cycles, changes in temperature and variations in soil moisture content.

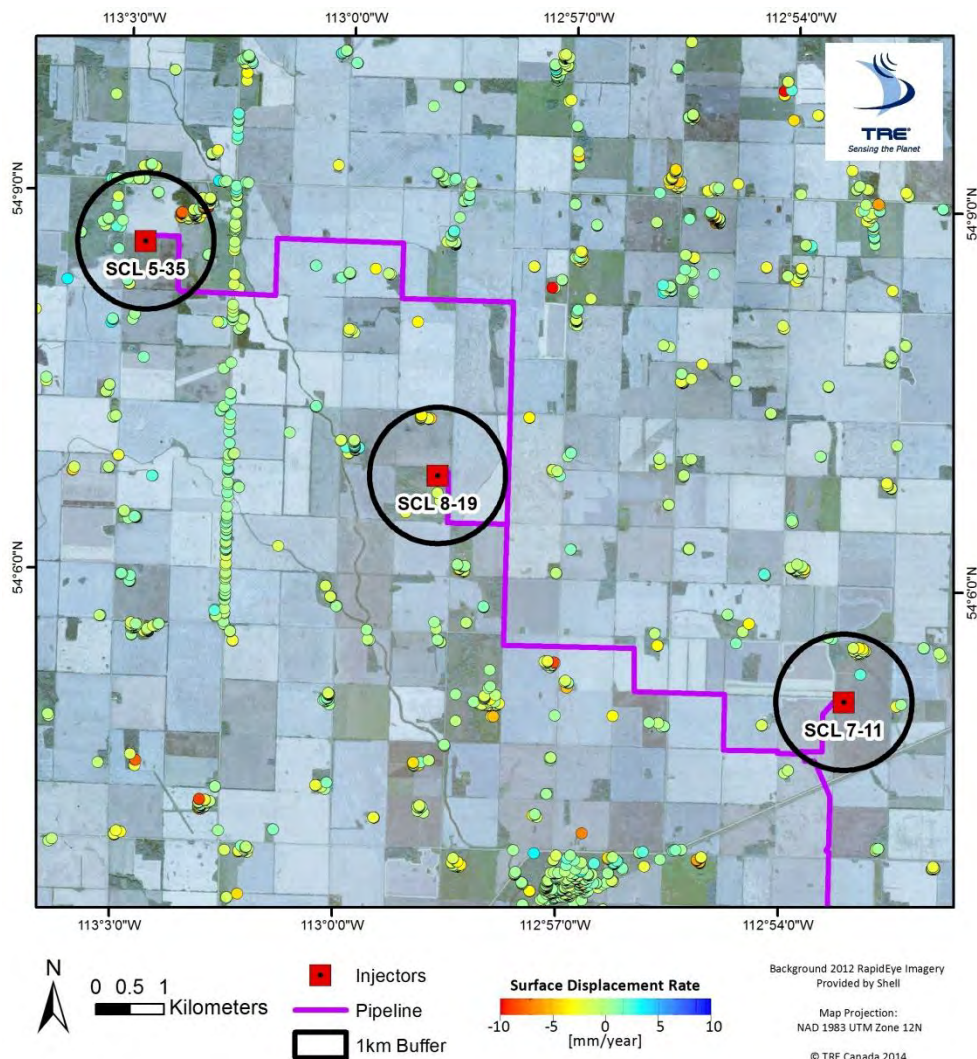


Figure 5: Close-up of the displacement results for the Quest proposed injection site.

Injection Well Full Name	Injection Well Short Name	Status	X Coord (m)	Y Coord (m)
100-08-19-059-20W4-00	SCL 8-19	Drilled	370,645.70	5,997,974.82
102-05-35-059-21W4-00	SCL 5-35	Drilled	366,359.88	6,001,418.03
103-07-11-059-20W4-00	SCL 7-11	Drilled	376,614.76	5,994,645.58

Table 2: Injection well locations over the Quest site.

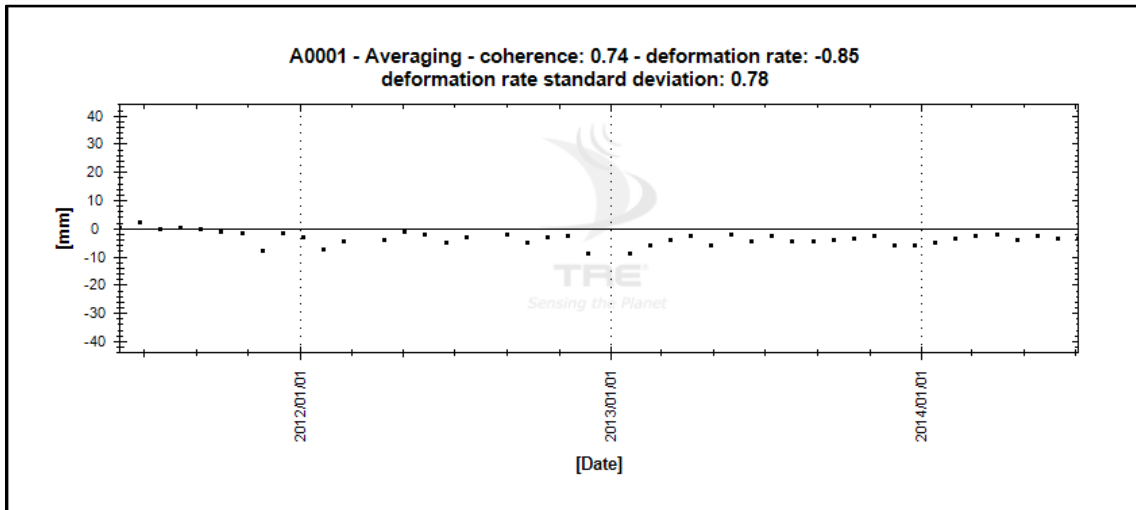


Figure 6: Average time series of measurement points identified within a 1 km buffer of well SCL 5-35 (shown in Figure 5).

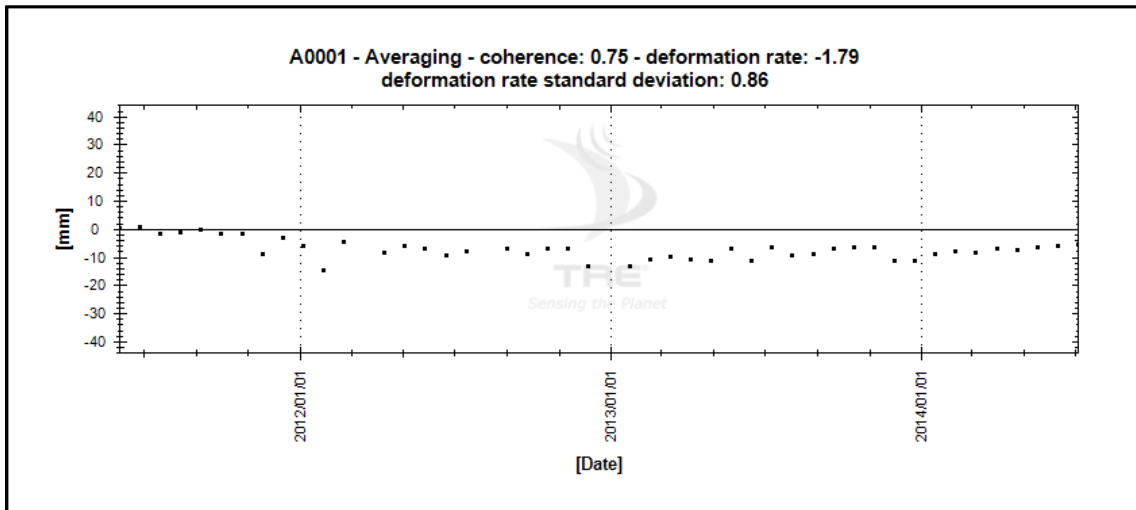


Figure 7: Average time series of measurement points identified within a 1 km buffer of well SCL 8-19 (shown in Figure 5).

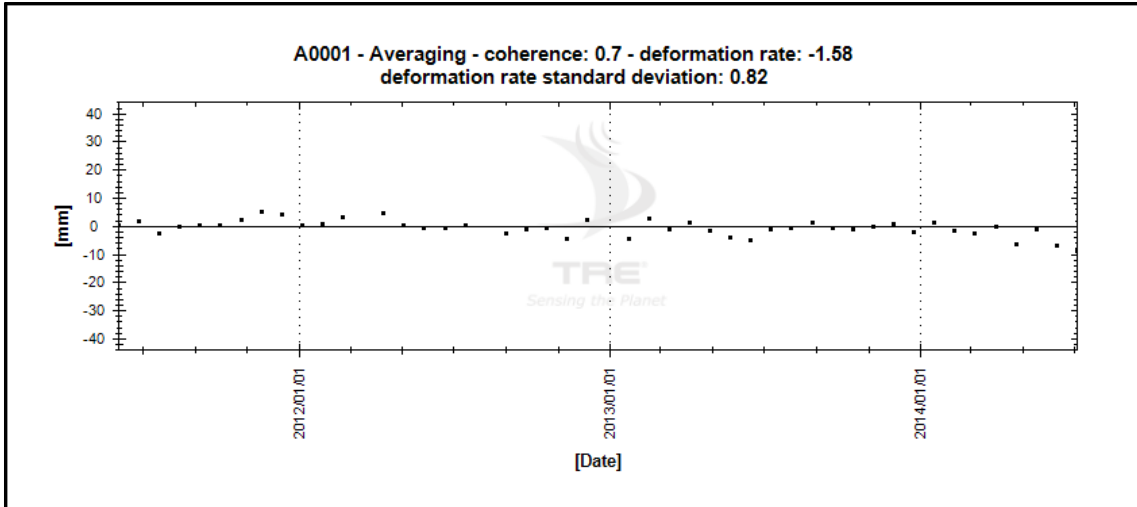


Figure 8: Average time series of measurement points identified within a 1 km buffer of well SCL 7-11 (shown in Figure 5).



## 6.2 Comparison of Results

Results obtained from the initial baseline analysis and the current processing are shown in Figure 9. An additional 14,369 measurement points were identified in the current analysis, primarily due to the processing of a larger data stack spanning a longer period of time (Table 3). The average standard deviation value of the surface displacement data has also decreased by more than half (from  $\pm 2.02$  mm/year to  $\pm 0.87$  mm/year) with the addition of more imagery. A density of 14.47 PS and DS per square kilometre was obtained from the updated data set, with a distribution of radar targets that is fairly consistent with the previous analysis. The main differences regard a lower density of points in the far northern portion of the AOI and a higher density in the western and southwestern section.

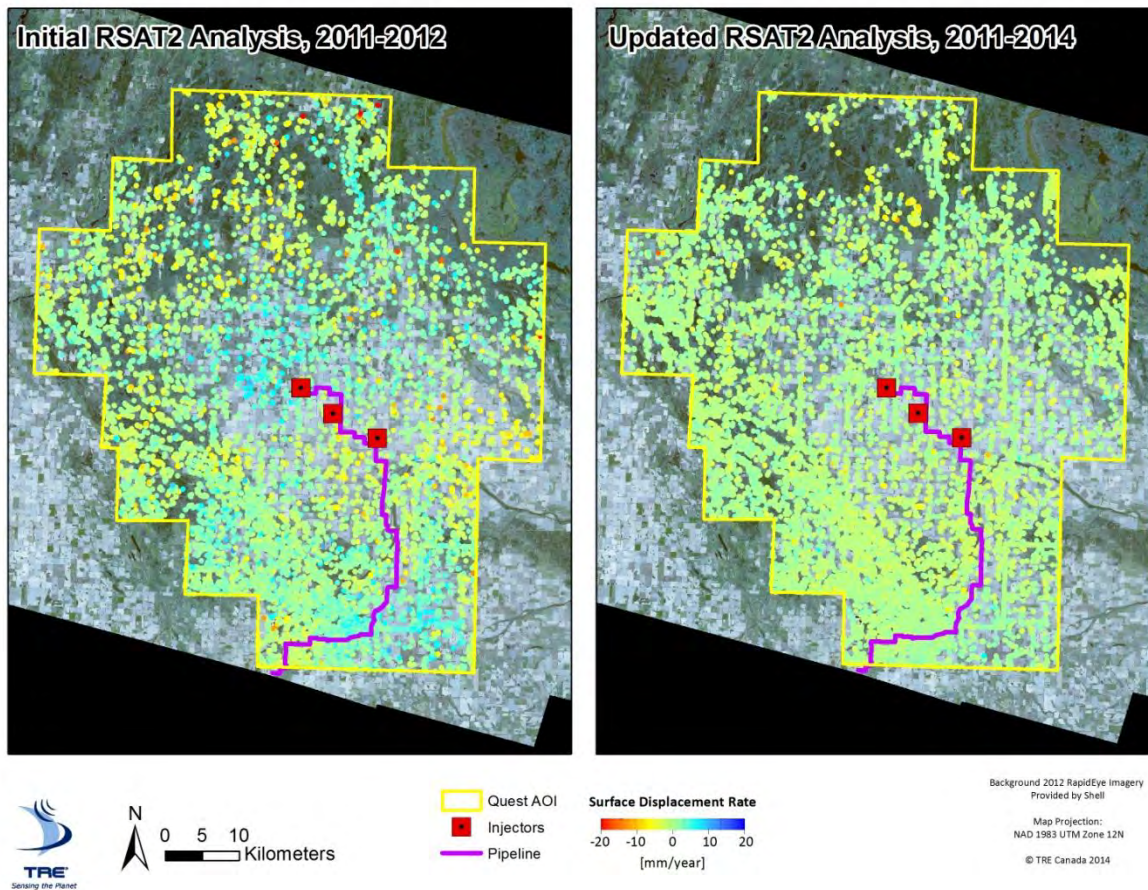


Figure 9: Surface displacement results obtained from the initial (left panel) and updated (right panel) analysis of the Radarsat-2 image stack.

Attribute	ERS Historical Analysis	Radarsat-2 First Analysis	Radarsat-2 Second Analysis
No. of images processed	33	22	45
Time period covered (years)	8.5	1.5	3
No. of PS	268	17,753	30,892
No. of DS	1,275	22,145	23,375
Total No. of Measured Points (PS and DS)	1,543	39,898	54,267
Average PS and DS (per square km)	0.41	10.64	14.47
Average Displacement Rate (mm/year)	-0.96	0.34	-0.22
Average Displacement Rate Standard Deviation (mm/year)	0.69	2.02	0.87

Table 3: Statistics of the historic ERS and baseline RSAT2 SqueeSAR analyses conducted over the Quest site.

### 6.3 Target Distribution and Density around Injection Wells

The distribution of measurement points identified around the three injection wells was examined to assess data coverage around critical operation zones. The number of points identified within these zones is summarized according to a 2 km x 2 km and 1 km x 1 km grid overlain on the results, centered over each well.

TRE considers all points identified within the SqueeSAR analysis and delivered to Shell to be reliable as they have undergone careful quality controls using TRE's ISO-certified procedures. However, to provide a measure of the comparative quality of the remaining points they have been further classified based on their coherence.

Coherence is a measure of comparative quality and uses an index that ranges from 0 to 1 which is linked to the stability of the phase component of the radar signal. Coherence values change with each data processing as the statistics of each data set are different. In general, as the number of processed images increases the average coherence over a site often decreases slightly. This is caused by the increased robustness of the statistical calculations used to identify measurement points, which allows coherence values to be reduced to include more points. While coherence values for the present update are slightly lower compared to the initial baseline analysis, the overall robustness of the results has increased due to the larger number of images covering a longer period of time. As a result, more points are now considered reliable, despite their marginally lower coherence values.

All measurement points were grouped into three classes according to their coherence values. For the present analysis, points with a value between 0.56 - 0.67 are classified as having "moderate" coherence, points in which values range between 0.68 – 0.82 are labeled as having "high" coherence and the remaining points, in which the values are greater than 0.83, are considered as having "very high" coherence.

### 6.3.1 Injector SCL 5-35

A total of 1,126 measurement points were identified within the 10 km x 10 km grid centered on injector SCL 5-35 (Figure 10). The density of PS and DS has increased from 7.54 points per square kilometre identified in the first baseline analysis, to 11.26 points per square kilometre. The total number of PS and DS found within each cell of the 2 km x 2 km grid and of the 1 km x 1 km grid is shown in Table 4 and Table 5, respectively.

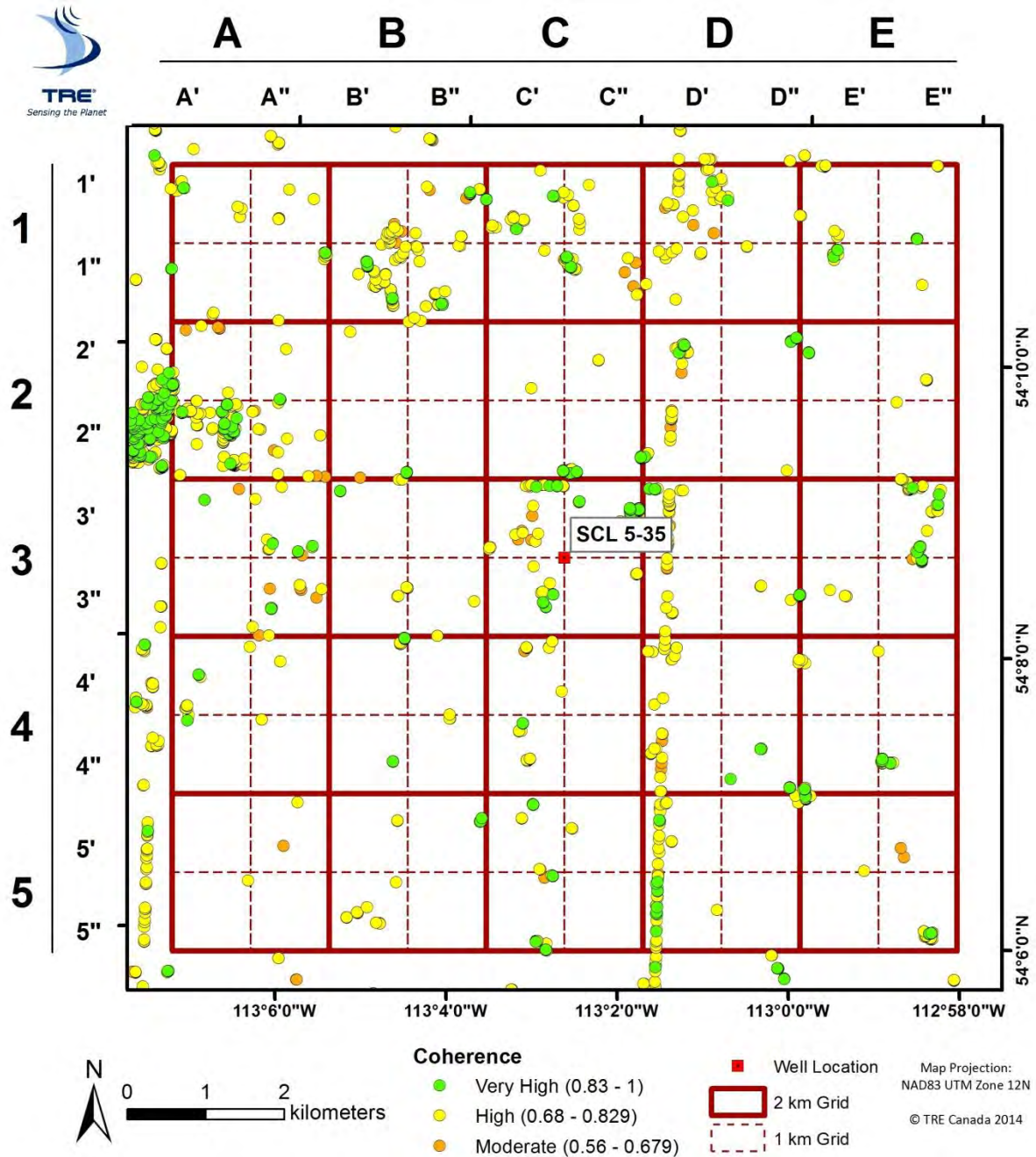


Figure 10: PS and DS measurement points comparatively classified based on their coherence values within 5 km of injector SCL 5-35.



**2 km x 2 km**

	<b>A</b>	<b>B</b>	<b>C</b>	<b>D</b>	<b>E</b>
<b>1</b>	28	107	59	51	29
<b>2</b>	183	7	31	45	11
<b>3</b>	31	15	139	49	59
<b>4</b>	17	19	24	42	29
<b>5</b>	3	19	31	47	50

Table 4: Density of PS and DS within each cell of the 2 km x 2 km grid centered over injector SCL 5-35.

**1 km x 1 km**

	<b>A'</b>	<b>A''</b>	<b>B'</b>	<b>B''</b>	<b>C'</b>	<b>C''</b>	<b>D'</b>	<b>D''</b>	<b>E'</b>	<b>E''</b>
<b>1'</b>	11	6	16	15	25	7	31	6	12	6
<b>1''</b>	2	9	49	27	2	25	12	2	10	1
<b>2'</b>	16	4	1	0	1	2	19	10	4	6
<b>2''</b>	147	16	6	0	4	24	15	1	0	1
<b>3'</b>	3	13	5	0	28	95	29	0	0	42
<b>3''</b>	0	15	7	3	13	3	11	9	4	13
<b>4'</b>	12	1	13	1	10	0	15	2	3	0
<b>4''</b>	2	2	3	2	14	0	15	10	9	17
<b>5'</b>	0	2	2	5	8	2	18	3	17	2
<b>5''</b>	1	0	12	0	21	0	26	0	0	31

Table 5: Density of PS and DS within each cell of the 1 km x 1 km grid centered over injector SCL 5-35.

### 6.3.2 Injector SCL 8-19

A total of 1,112 measurement points were identified within the 10 km x 10 km grid centered on injector SCL 8-19 (Figure 11). The density of PS and DS has increased from 8.38 points per square kilometre identified in the first baseline analysis, to 11.12 points per square kilometre. The total number of PS and DS found within each cell of the 2 km x 2 km grid and of the 1 km x 1 km grid is shown in Table 6 and Table 7, respectively.

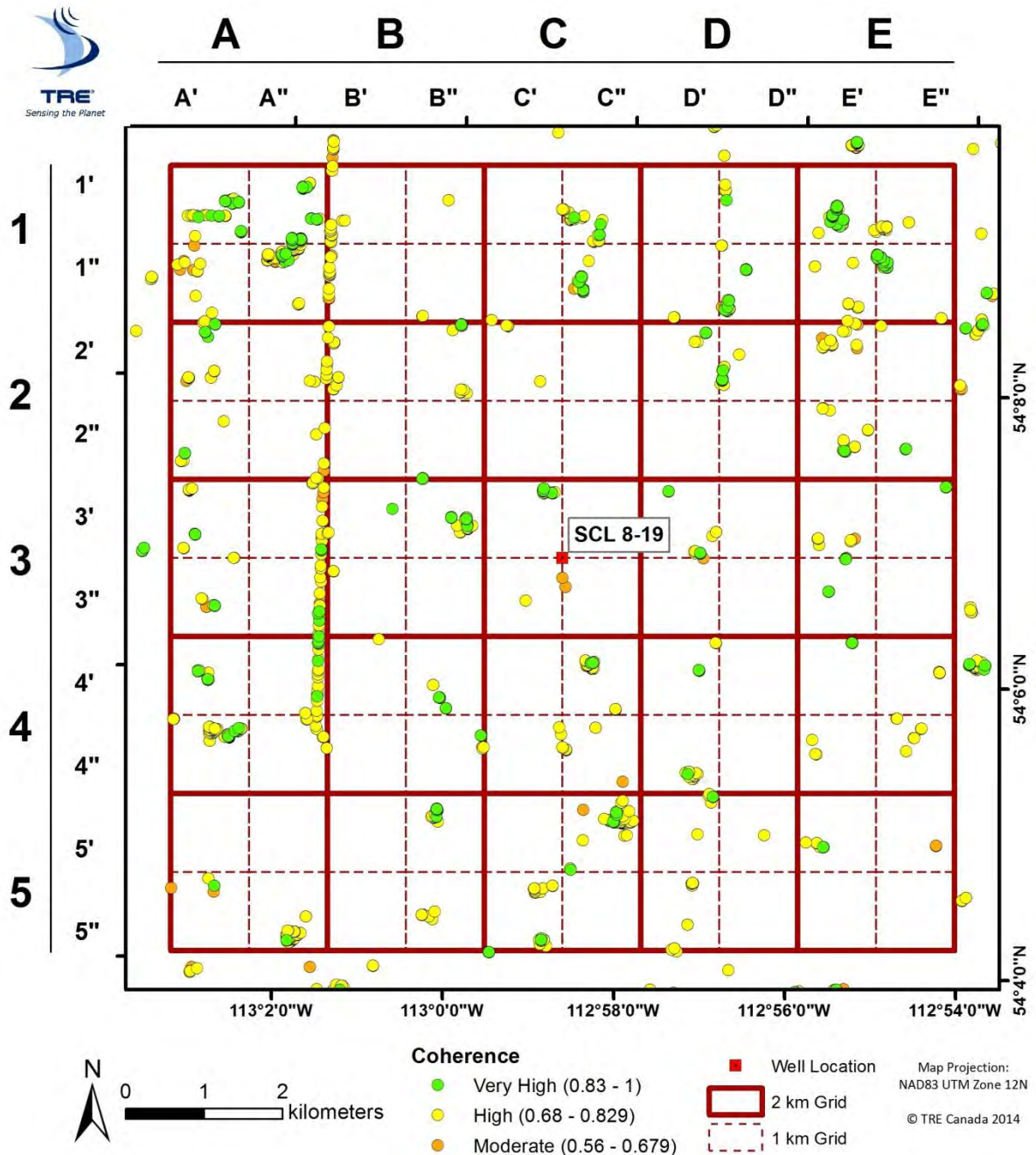


Figure 11: PS and DS measurement points classified based on their coherence values within 5 km of injector SCL 8-19.

**2 km x 2 km**

	<b>A</b>	<b>B</b>	<b>C</b>	<b>D</b>	<b>E</b>
<b>1</b>	176	29	56	37	122
<b>2</b>	45	26	4	22	40
<b>3</b>	60	37	20	14	19
<b>4</b>	125	19	45	23	23
<b>5</b>	50	28	70	21	9

**Table 6: Density of PS and DS within each cell of the 2 km x 2 km grid centered over injector SCL 8-19.**

**1 km x 1 km**

	<b>A'</b>	<b>A''</b>	<b>B'</b>	<b>B''</b>	<b>C'</b>	<b>C''</b>	<b>D'</b>	<b>D''</b>	<b>E'</b>	<b>E''</b>
<b>1'</b>	38	55	14	1	3	30	0	5	45	11
<b>1''</b>	14	69	12	2	1	22	3	29	9	57
<b>2'</b>	19	10	10	12	4	0	5	17	18	1
<b>2''</b>	8	8	0	4	0	0	0	0	18	3
<b>3'</b>	14	17	4	32	17	0	13	0	8	4
<b>3''</b>	10	19	1	0	2	1	1	0	7	0
<b>4'</b>	14	21	1	12	0	34	7	0	9	4
<b>4''</b>	75	15	0	6	4	7	16	0	3	7
<b>5'</b>	0	0	0	21	0	45	8	1	7	2
<b>5''</b>	6	44	0	7	25	0	12	0	0	0

**Table 7: Density of PS and DS within each cell of the 1 km x 1 km grid centered over injector SCL 8-19.**

### 6.3.3 Injector SCL 7-11

A total of 888 measurement points were identified within the 10 km x 10 km grid centered on injector SCL 7-11 (Figure 12). The density of PS and DS has increased from 6.98 points per square kilometre identified in the first baseline analysis, to 8.88 points per square kilometre. The total number of PS and DS found within each cell of the 2 km x 2 km grid and of the 1 km x 1 km grid is shown in Table 8 and Table 9, respectively.

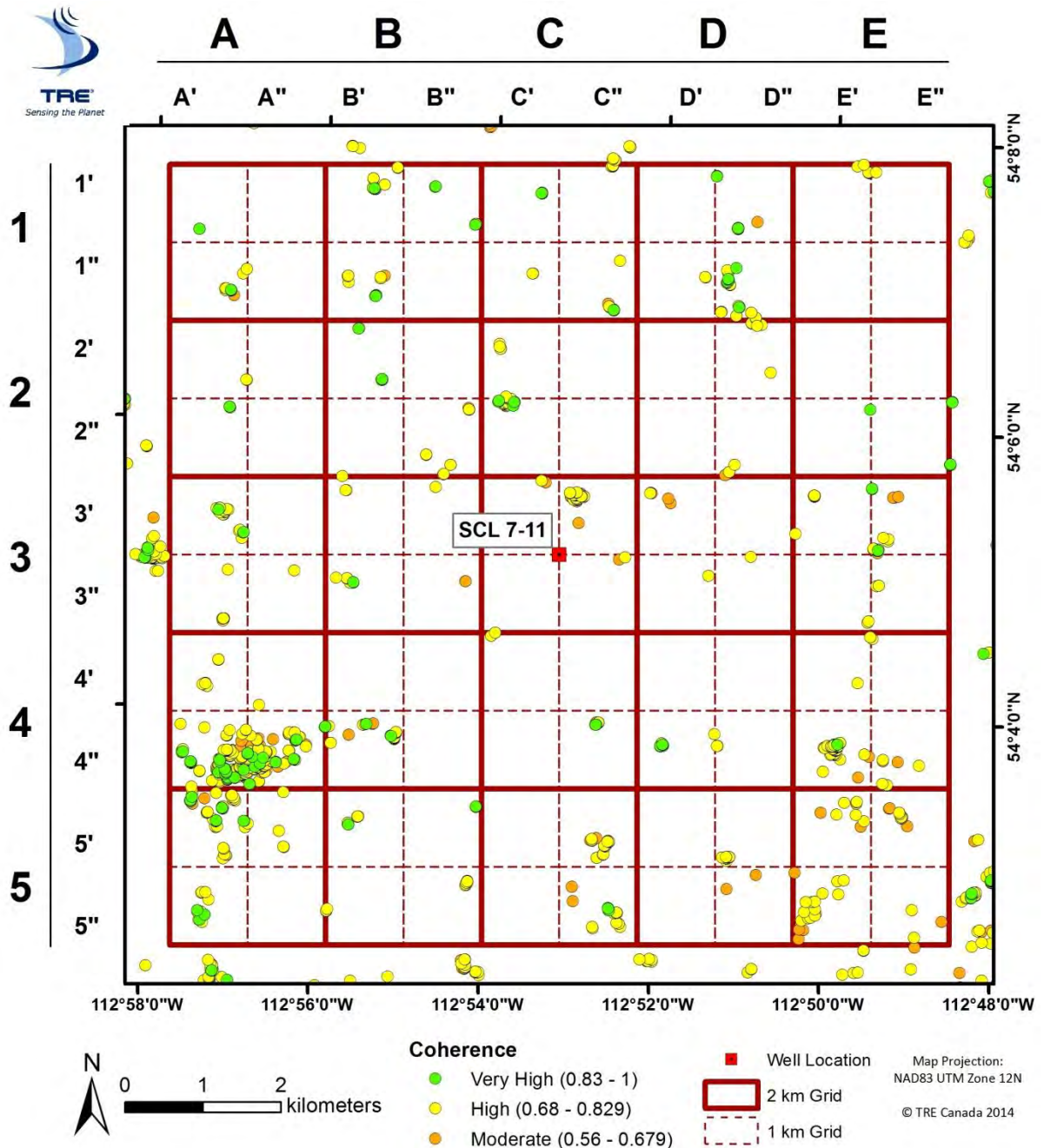


Figure 12: PS and DS measurement points classified based on their coherence values within 5 km of injector SCL 7-11.

**2 km x 2 km**

	<b>A</b>	<b>B</b>	<b>C</b>	<b>D</b>	<b>E</b>
<b>1</b>	13	34	20	37	7
<b>2</b>	7	23	33	11	1
<b>3</b>	31	12	37	7	35
<b>4</b>	304	23	11	13	51
<b>5</b>	69	19	35	13	42

**Table 8: Density of PS and DS within each cell of the 2 km x 2 km grid centered over injector SCL 7-11.**

**1 km x 1 km**

	<b>A'</b>	<b>A''</b>	<b>B'</b>	<b>B''</b>	<b>C'</b>	<b>C''</b>	<b>D'</b>	<b>D''</b>	<b>E'</b>	<b>E''</b>
<b>1'</b>	2	0	15	7	4	4	0	9	6	1
<b>1''</b>	11	0	12	0	2	10	2	26	0	0
<b>2'</b>	2	0	12	0	9	0	0	7	0	0
<b>2''</b>	5	0	1	10	24	0	0	4	1	0
<b>3'</b>	23	0	2	1	3	32	5	0	8	22
<b>3''</b>	7	1	7	2	0	2	1	1	2	3
<b>4'</b>	8	1	0	0	4	0	0	0	3	1
<b>4''</b>	176	119	23	0	0	7	11	2	40	7
<b>5'</b>	52	4	7	3	0	19	0	11	9	11
<b>5''</b>	13	0	3	6	0	16	0	2	19	3

**Table 9: Density of PS and DS within each cell of the 1 km x 1 km grid centered over injector SCL 7-11.**

## 7 Conclusions

The results of the updated InSAR analysis over the Quest Project site indicate that minimal ground displacement is occurring throughout the entire AOI. Mild fluctuations are present within some of the displacement time series which are likely linked to seasonal fluctuations.

In general, with the addition of more imagery collected over a longer period of time, the results of the present analysis have improved in comparison to the initial analysis conducted over this site. A larger number of points was identified over the entire AOI, the density of measurement points in the areas surrounding the three injection wells has increased by approximately 36%, on average, and the precision of the measurements has improved considerably, with confidence limits becoming sub-millimetric.



**TRE<sup>®</sup>**

*Sensing the Planet*

**TRE Canada Inc.  
475 West Georgia Street, Suite 410  
Vancouver, B.C., V6B 4M9  
Canada**

**Tel. 604 331-2512  
[www.trecanada.com](http://www.trecanada.com)**